The Astrophysical Journal, 578:194–210, 2002 October 10

COMPOSITION OF ANOMALOUS COSMIC RAYS AND OTHER HELIOSPHERIC IONS

A. C. Cummings, E. C. Stone, and C. D. Steenberg
California Institute of Technology, Pasadena, CA 91125
Received 2002 April 3; accepted 2002 June 20

ABSTRACT

Interstellar pickup ions accelerated by the termination shock of the solar wind dominate the anomalous cosmic-ray (ACR) intensities observed by the *Voyager* spacecraft in the outer heliosphere. Using a two-dimensional acceleration and propagation model, we derive the relative abundances of these interstellar ACRs and determine the mass dependence of the injection/acceleration efficiency for the diffusive acceleration of H^+, He^+, N^+, O^+, and Ne^+. The energy spectra of C, Na, Mg, Si, S, and Ar also exhibit ACR increases at low energies. To interpret these observations, we have developed a new set of ionization rates for 11 neutral atoms, H, He, C, N, O, Ne, Na, Mg, Si, S, and Ar at 1 AU, and a new set of filtration factors relating neutral densities in the local interstellar medium to those at the location of the solar wind termination shock. Using the injection/acceleration efficiencies and the Ar filtration factor, we estimate the density of neutral Ar to be $(3.5 \pm 1.6) \times 10^{-7}$ cm^{-3} in the local interstellar medium. ACR C may have a significant contribution from interstellar neutral C, but the observed intensities of ACR Na, Mg, Si, and S significantly exceed that expected from interstellar neutrals, providing evidence of another source of pickup ions. One possibility discussed is the recently discovered "inner source" of singly charged ions that is thought to be solar wind atoms desorbed from interplanetary dust grains.

Subject headings: acceleration of particles — atomic processes — cosmic rays — interplanetary medium — ISM: abundances — ISM: atoms

On-line material: color figures

1. INTRODUCTION

Anomalous cosmic rays (ACRs) are traditionally defined as those particles in the energy spectra of cosmic rays that originate as interstellar neutral gas flowing into the heliosphere (Fisk, Kozolovsky, & Ramaty 1974), become ionized, and are eventually accelerated at the solar wind termination shock (Pesses, Jokipii, & Eichler 1981). As a result, the ACRs at low energies are mostly singly charged particles (Klecker et al. 1995).

The composition of this component thus bears on a number of astrophysical questions, such as the abundance of interstellar neutrals, the ionization state of the local interstellar medium, the fractionation in the abundances that occurs in the heliosheath, in the interplanetary ionization process, and in the injection, acceleration, and interplanetary propagation processes.

The most abundant species of the ACR component are the elements that occur with reasonably high abundance in the neutral gas of the very local interstellar medium (VLISM). Neutral particles flow into the heliosphere because they are not deflected by the heliospheric magnetic field. The abundant ACR elements all have first ionization potentials (FIPs) greater than or equal to that of H, and all have been observed in the outer heliosphere: H, He, N, O, Ne, and Ar (Cummings & Stone 1998), and all but H have been observed in the inner heliosphere as well (Klecker et al. 1998; Reames 1999; Leske et al. 2000).

Recent observations at 1 AU with the *Wind* spacecraft and in the outer heliosphere with the *Voyager* spacecraft have revealed intensity increases at low energies of other ions, such as Mg, Si, and S (Takashima et al. 1997; Reames 1999; Stone & Cummings 1997; Cummings, Stone, & Steenberg 1999). The origin of these low-energy intensity increases of ions with low FIP has been attributed to the interstellar ACR component (Stone & Cummings 1997), as well as to reaccelerated solar wind (Mewaldt 1999). Recently, Gloeckler et al. (2000b) have suggested that the recently observed inner source pickup ions may be the seed particles for this ACR component.

Recent observations with the *SAMPEX* spacecraft show that at ~350 MeV, ACR N and O ions at 1 AU transition from being mostly singly charged at lower energies to multiply charged at higher energies (Klecker et al. 1995; Mewaldt et al. 1996; Jokipii 1996; Barghouty et al. 2000). The multiply charged ions have been attributed to charge-stripping as the particles are accelerated at the solar wind termination shock and interact with the inflowing neutral interstellar H and He. Recently, the relevant charge-stripping cross sections have been calculated (Barghouty 2000; Barghouty et al. 2001).

In this paper we compare cosmic-ray observations from the *Voyager* and *Wind* spacecraft with the results from a two-dimensional numerical model of ACR acceleration and propagation and galactic cosmic-ray (GCR) propagation that incorporates the charge-stripping effect for ACRs. We fit the model to energy spectra acquired during the current solar minimum period of 11 elements: H, He, C, N, O, Ne, Mg, Na, Si, S, and Ar. The energy spectra in the outer heliosphere are from the Cosmic Ray experiment on each of *Voyagers 1* (*V1*) and *2* (*V2*) (Stone et al. 1977). The observations at 1 AU are taken from Reames (1999). We produce a new table of the abundances and relative injection/acceleration efficiencies of the high-FIP ions. We also estimate the neutral density of Ar in the VLISM and investigate possible origins for the low-FIP ions in the outer heliosphere.

2. SELECTION OF TIME PERIODS FOR ANALYSIS

In Figure 1 we show yearly averaged energy spectra of cosmic-ray H and He obtained by the Cosmic Ray experiment on *V1* and *V2*. Above ~100 MeV nucleon^{-1} the energy spectra are dominated by GCRs. The intensity of these particles is seen to increase by a factor of ~2–3 from 1993 through 1999. Below ~100 MeV nucleon^{-1}, the energy spectra are dominated by ACRs over most of the time period. The intensity variation is much larger than in the GCRs.

In the top two panels of Figure 2 we show the time profiles of the intensity near the peak of the energy spectra of ACR H and He from 1993/3 to 2000/218. The intensities increase by a factor of nearly 100 from early 1993 until reaching a plateau near the beginning of 1998. The intensities, particularly at *V2*, show a significant decrease near mid-2000. In the bottom panel of Figure 2 we show the time profile of ACR oxygen with 7.1–17.1 MeV nucleon^{-1}. The intensity in this part of the energy spectrum, which is well above the peak energy (Hamilton et al. 1999), changes relatively little over the period shown.

We define the current solar minimum period as 1998/1–1999/182, corresponding to the plateau period in the top two panels of Figure 2. This is a period in which the ACR H and He energy spectra have stopped evolving and thus represents an equilibrium period for these particles in the heliosphere.

This relatively short solar minimum period is adequately long to define the energy spectra of the abundant ACRs. However, to investigate the energy spectra of the rarer, low-FIP ions, a longer period is desirable. For these ions we choose the period 1993/53–1999/365 to construct energy spectra. Fortunately, the observations of these low-FIP ions occur at relatively high energies compared to the energy of their peak intensity, so limited evolution of the observed energy spectra is expected over this longer time period.

3. THE ACCELERATION AND PROPAGATION MODEL

The acceleration and propagation model is based on the two-dimensional time-dependent solution of the cosmic-ray transport equation (TPE) of Steenkamp (1995), with the addition of accounting for charge-stripping of the ions, as described in Jokipii (1996) and Steenberg (2000). The TPE for ionization state $i > 0$ is given by

$$\frac{\partial f_i}{\partial t} = \nabla \cdot (\mathbf{K}_i \cdot \nabla f_i - \boldsymbol{V} f_i) + \frac{1}{3P^2}(\nabla \cdot \boldsymbol{V})\frac{\partial}{\partial P}(P^3 f_i) + Q_i \qquad (1)$$

where f_i is the omnidirectional distribution function, $\mathbf{K}_i$ is the diffusion tensor, P is the particle rigidity, $\boldsymbol{V}$ is the solar wind velocity, and the source term is $Q_i = Qs + n_{\rm H} C_{\rm He}[R_{i-1}(E) f_{i-1} - R_i(E) f_i]$, where $Q_s = Q_0 \delta(r - r_s)\delta(P - P_0)$ and E is energy per nucleon. The neutral hydrogen collision ionization rate is given by $R_i = \sigma_i(E) w$, where w is the particle speed relative to the neutral hydrogen and $\sigma_i(E)$ is the neutral hydrogen ionization cross section. The factor $C_{\rm He} = [1 + (Z^2 n_{\rm He}/n_{\rm H})] \exp[-(3Z\alpha^2/2\beta^2)]$ accounts for additional ionization by neutral He (Barghouty et al. 2001), with $Z = 2$, $\alpha \approx 1/137$, the fine-structure constant, and $\beta = w/c$ the speed of the ACR ion. The addition of stripping by neutral helium collisions increases the ionization rates by

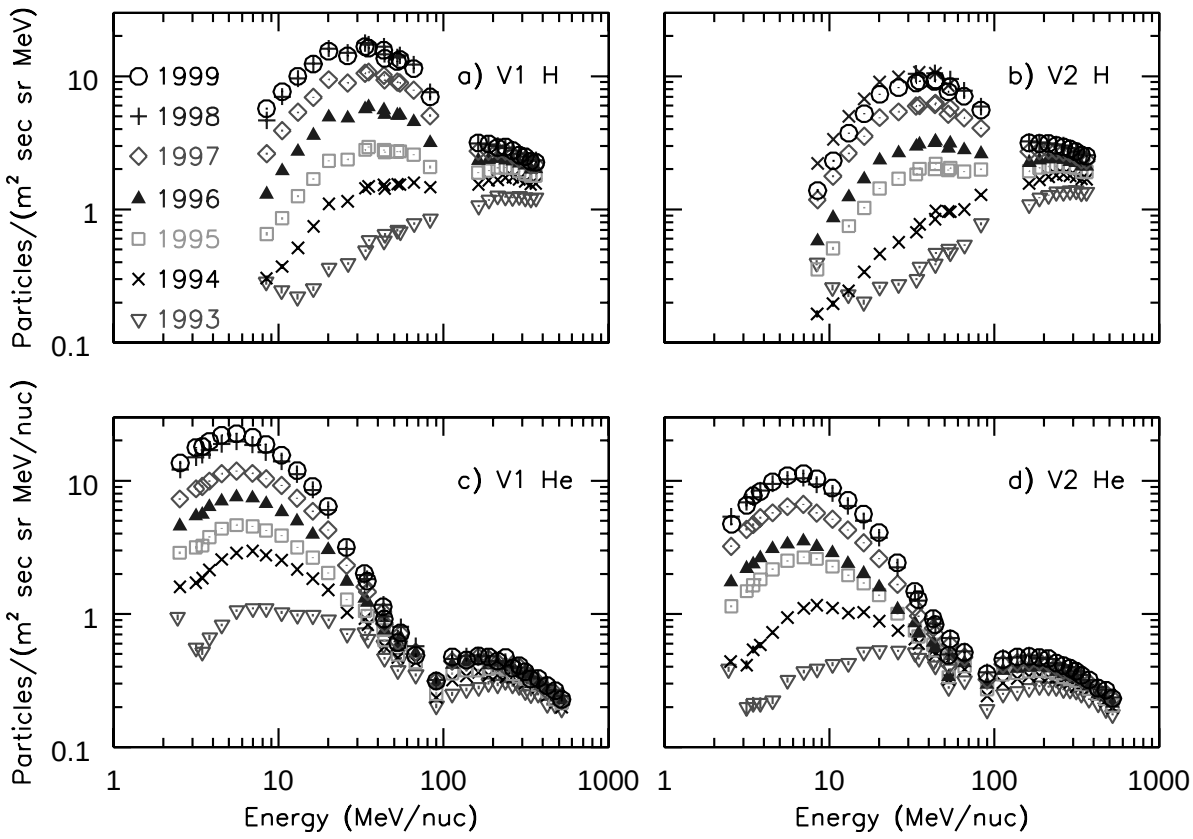

FIG. 1.—Yearly averaged energy spectra of cosmic-ray H and He at *V1* and *V2* for 1993–1999. At energies above ~100 MeV nucleon^{-1} for H and He, there exist unresolved systematic uncertainties of ~15%. [*See the electronic edition of the Journal for a color version of this figure.*]

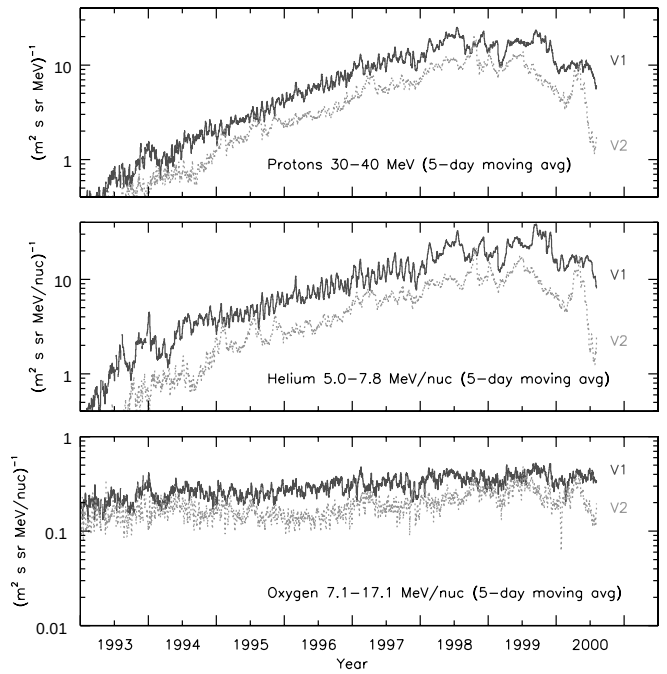

FIG. 2.—Five-day moving averages of the intensities of protons (*top*), helium (*middle*), and oxygen (*bottom*). [*See the electronic edition of the Journal for a color version of this figure.*]

up to 85% at higher energies (~30 MeV nucleon^{-1} ACR oxygen) relative to stripping by neutral hydrogen alone.

Calculations of energy spectra at the shock, at 1 AU, and at the positions of the *V1* and *V2* spacecraft were made for three cases: the short solar minimum period (1998/1–1999/182) for both a strong shock (shock strength $s = 4$) and weak shock ($s = 2.4$) and the long period (1993/53–1999/365) for a strong shock. For the strong shock cases, identical parameter sets were used with the shock placed at 90 AU. For the weak shock case, the diffusion coefficient was modified and the shock was placed at 110 AU.

Singly charged ions are initially injected at the solar wind termination shock at 10 keV nucleon^{-1} for the strong shock case and ~100 keV nucleon^{-1} for the weak shock case. These ions undergo acceleration at the termination shock as well as ionization due to collisions with heliospheric neutral hydrogen and helium, in addition to the well-known modulation processes of convection, diffusion, adiabatic energy losses, and drift. The TPE is solved for each ionization state, with collision cross sections calculated by Barghouty (2000) and Barghouty, Jokipii, & Mewaldt (2001), using neutral hydrogen and helium densities of 0.084^{-3} and 0.018 cm^{-3}, respectively, similar to values derived by Gloeckler & Geiss (2001) from *Ulysses* pickup ion observations.

Numerical solutions of the TPE are obtained for 140 radial intervals between a reflecting inner boundary at $r_i = 0.05$ AU and outer free escape boundary $r_b = 200$ AU. A latitudinal grid of 31 equally spaced points was used, assuming symmetry around the heliographic equatorial plane. The solar wind speed is $V(r, \theta) = 400j(r)k(\theta)$ km s^{-1}. The solar wind has a latitudinal dependence given by $k(\theta) = 1.5 + 0.5 \cos[\pi(\theta - 40^\circ)/50^\circ]$ for polar angle theta between 40° and 140°. Within 40° of either pole, $k(\theta) = 2.0$. This functional form agrees reasonably well with *Ulysses* observations (see, e.g., Goldstein et al. 1995).

TABLE 1

AVERAGE *Voyager* SPACECRAFT HELIOGRAPHIC LOCATIONS

	V1		*V2*	
PERIOD	Radius (AU)	Latitude (deg)	Radius (AU)	Latitude (deg)
1998/1–1999/182.....	71.6	33.3	56.0	−19.4
1993/53–1999/365.....	63.7	32.8	49.6	−14.8

A diffusion mean free path length of $\lambda_{rr} = 3\kappa_{rr}/w = h(P)e(r)g(\theta)$ AU was specified; $\lambda_{\theta\theta}$ was set to 0.5 of λ_{rr} everywhere, and w is the particle speed in the rest frame of the Sun. The latitudinal dependence of the mean free path length is given by $g(\theta) = 1.5 + 0.5 \cos[\pi(0/90^\circ)]$, where θ is the polar angle.

The same radial dependence was used for λ_{rr} and $\lambda_{\theta\theta}$ and consisted of five power-law segments. Between 85 and 90 AU for the strong shock case and between 104 and 110 AU for the weak shock case, we assumed that there was increased magnetic turbulence associated with upstream waves from the shock. The terms λ_{rr} and $\lambda_{\theta\theta}$ decreased by a factor of 5 in this region, with a further factor of 4 decrease at the shock itself. The radial, rigidity, and latitudinal dependences of the solar wind speed and mean free path length for the strong and weak shock cases are shown in Figure 3.

A monoenergetic spectrum of particles is injected at a rigidity P_0, with the rigidity domain divided into 497 logarithmically spaced intervals for ACRs. For the GCR runs, a coarser grid of 88 logarithmically spaced intervals was used. The model is run for a total of 9.7 yr. A Jokipii-Kóta modified Parker spiral field (Jokipii & Kóta 1989) was specified, with a field strength of $B_e = 5$ nT at Earth and a simulated neutral sheet with a tilt angle of 15°. The modification increases the magnetic field strength by a factor of 10 over the poles.

For GCR calculations, a local interstellar spectrum of

$$j(r_b, \theta, P) = \frac{Zj_0\beta P}{A(E + 0.5E_0)^{3.6}} \quad (2)$$

was specified at $r_b = 200$ AU, where E is the energy per nucleon in GeV nucleon^{-1}, P is the rigidity in GV, $E_0 = 0.938$ GeV, and j is the differential intensity. The values of j_0 were determined from least-squares fits to the data.

Energy spectra are calculated for 1 AU in the heliographic equatorial plane and for the average positions of the *Voyager* spacecraft in the two periods 1998/1–1999/182 and 1993/53–1999/365. The average *Voyager* locations for the two time periods are given in Table 1.

4. HIGH-FIP IONS: INTERSTELLAR ACRs

4.1. *Relative Abundances*

The energy spectra obtained at *V1* and *V2* for H, He, N, O, Ne, and Ar for the solar minimum period 1998/1–1999/182 are shown in Figure 4. These elements all have FIPs at or above that of H (13.6 eV) and are expected to occur with reasonably high abundance as neutral gas in the local interstellar medium (Frisch 1998). Thus these elements are able to penetrate into the heliosphere as neutrals, become ionized, and are subsequently accelerated to energies where

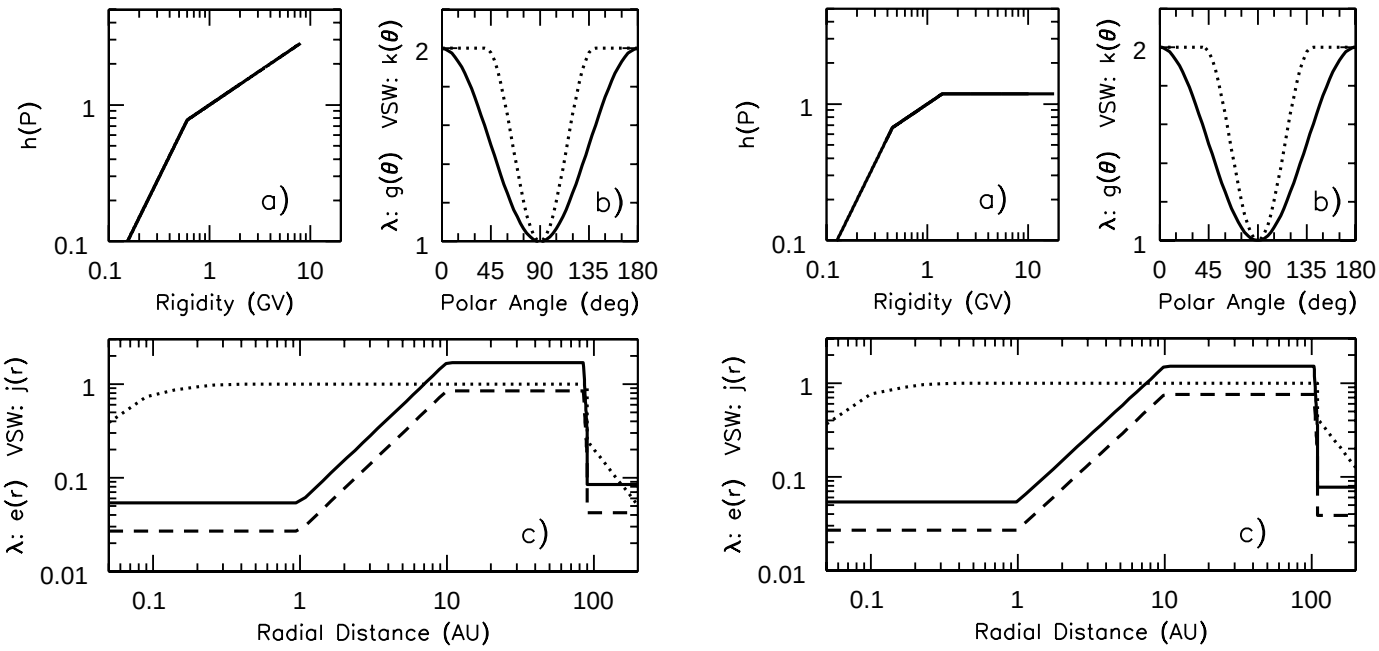

FIG. 3.—Solar wind speed [$V(r,\theta) = 400j(r)k(\theta)$ km s^{-1}] and mean free path length [$\lambda_{rr}, \lambda_{\theta\theta} = h(P)e(r)g(\theta)$ AU] for the strong shock case (*left-hand panels*) and the weak shock case (*right-hand panels*). (*a*) Rigidity dependence of λ_{rr} and $\lambda_{\theta\theta}$. (*b*) Polar angle dependence of λ_{rr} and $\lambda_{\theta\theta}$ (*solid line*) and solar wind speed (*dotted line*). (*c*) Radial dependence of λ_{rr} (*solid line*), $\lambda_{\theta\theta}$ (*dashed line*), and solar wind speed (*dotted line*).

they are observed as ACRs (greater than a few MeV nucleon^{-1}).

All of the energy spectra in Figure 4 show an increase at low energies due to ACRs. In the case of H, the ACR component peaks at ~30–40 MeV, with an additional increase below ~5 MeV that is likely due to a local interplanetary acceleration process associated with corotating interaction regions (CIRs). Also shown in the left-hand panels of Figure

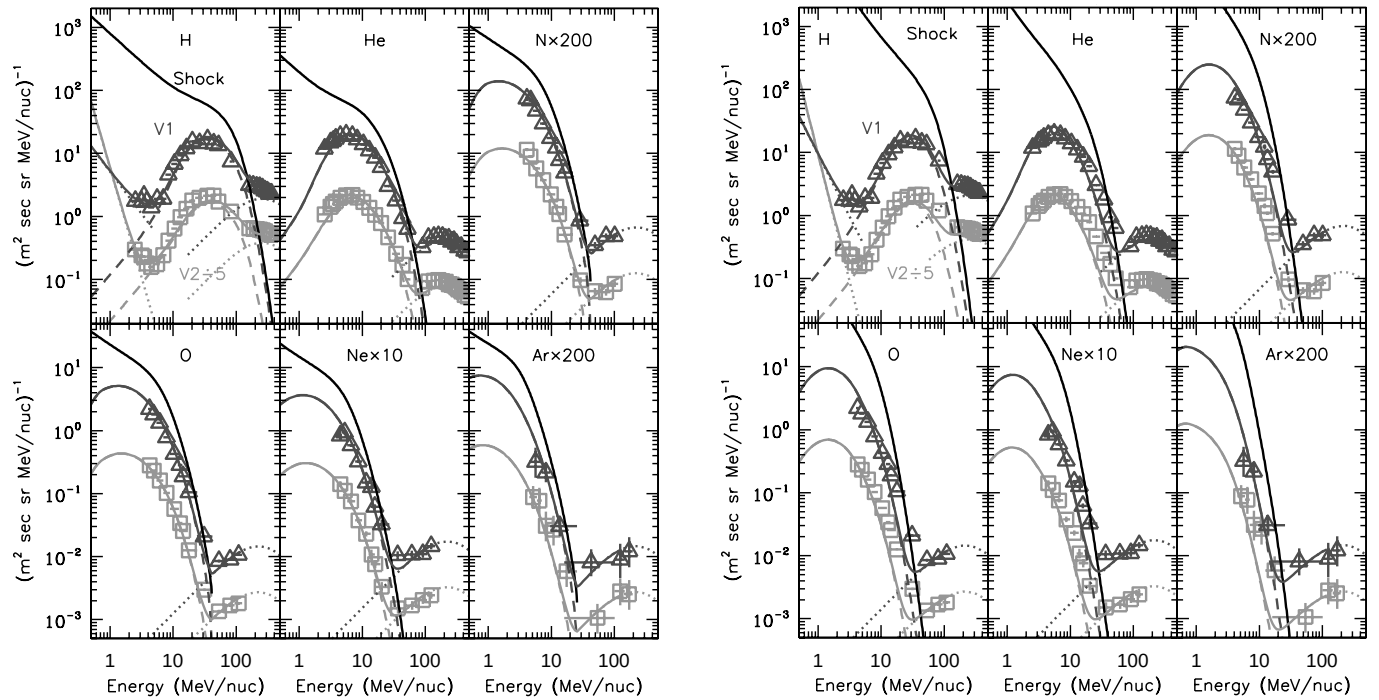

FIG. 4.—Energy spectra of six high-FIP ACR ions at *V1* (*triangles*) and *V2* (*squares*) for 1998/1–1999/182 from the CRS experiment. The left-hand panels show model fits for the strong shock case, and the right-hand panels show model fits for the weak shock case. In some panels factors are shown that have been applied to the *V1* observations before plotting. The *V2* observations use the same factors for *V1* plus an additional factor of 0.2 for clarity purposes. The solid curves through the data points are model calculations fitted to the sum of ACRs and GCRs as described in the text. In the case of H, an additional low-energy power-law component has been added. The upper solid curve is the ACR spectrum at the shock at 90 AU at a polar angle of 30°. [*See the electronic edition of the Journal for a color version of this figure.*]

TABLE 2
ABUNDANCES OF ACRs (RELATIVE TO He) AT THE SOLAR WIND TERMINATION SHOCK[a]

Element	Strong Shock ($s = 4$)	Weak Shock ($s = 2.4$)
H	4.17 ± 0.20	5.18 ± 0.24
He	1.00[b]	1.00[c]
N	$(1.48 \pm 0.07) \times 10^{-2}$	$(1.56 \pm 0.08) \times 10^{-2}$
O	$(1.03 \pm 0.05) \times 10^{-1}$	$(1.04 \pm 0.06) \times 10^{-1}$
Ne	$(6.68 \pm 0.37) \times 10^{-3}$	$(6.57 \pm 0.41) \times 10^{-3}$
Ar	$(5.18 \pm 0.94) \times 10^{-4}$	$(6.56 \pm 0.13) \times 10^{-4}$

[a] Derived from *V1* and *V2* observations for the period 1998/1–1999/182.
[b] Actual intensity at shock at 0.5 MeV nucleon^{-1} = $(3.59 \pm 0.10) \times 10^2$ (m^2 s sr MeV nucleon^{-1})$^{-1}$.
[c] Actual intensity at shock at 0.5 MeV nucleon^{-1} = $(6.97 \pm 0.21) \times 10^3$ (m^2 s sr MeV nucleon^{-1})$^{-1}$.

4 are fits to the data of the model calculations of ACR and GCR energy spectra described above assuming a shock compression ratio, s, of 4.0 (strong shock case). In the case of H, an additional low-energy power-law CIR component was included in the fit. For all data, an assumed systematic uncertainty of 15% was added in quadrature to the statistical uncertainties before fitting. Only the statistical uncertainties are shown in the figure.

The ACR spectra at the solar wind termination shock at 90 AU at a polar angle of 30° are also shown. Note that the spectra at the shock all have a power-law portion at the lowest energies and roll over to a very steep spectrum at high energies. The power-law index, γ, is related to the shock strength, s (see, e.g., Blandford & Ostriker 1978), by $\gamma = (s + 2)/(2 - 2s)$, and is thus -1 for $s = 4$. Comparing intensities at a common energy per nucleon in the power-law regime is a measure of the relative abundance of the diffusively accelerated ACR ions. For this study, we choose 0.5 MeV nucleon^{-1} as the comparison energy.

The model spectra for the strong shock fitted the *Voyager* spectra quite well. However, the fit is sensitive to the characteristics of the spectrum at the shock such as the roll-off at high energies. To illustrate the sensitivity of the derived relative abundances to the spectra at the shock, we show in the right-hand panels of Figure 4 similar fits to the *V1* and *V2* data assuming a weak shock with a compression ratio $s = 2.4$. These spectral fits are not as good as those with the strong shock for these particular model parameters. However, the abundances at the shock relative to He differ by $\lesssim 25\%$ from the strong shock case (Table 2), even though the intensities of the spectra at the shock for the weak and strong shock cases at 0.5 MeV nucleon^{-1} differ by a factor of ~ 20.

4.2. *Acceleration Efficiency*

We can use these observations together with observations of pickup ions to infer the efficiency, ϵ_i, for the injection and diffusive acceleration of pickup ion species i relative to He (referred to hereafter in this paper as the acceleration efficiency):

$$\epsilon_i = (j_i/j_{\rm He})/(F_i/F_{\rm He}) \, , \qquad (3)$$

where j_i is the intensity of the ith ACR element at the shock (polar angle 30°) at 0.5 MeV nucleon^{-1} and F_i is the flux of pickup ions of the ith element flowing into the nose of the shock. The ratios $j_i/j_{\rm He}$ are given in Table 2. The pickup ion fluxes at the shock can be estimated from the inferred neutral densities in the outer heliosphere (Gloeckler & Geiss 2001), ionization rates at 1 AU (derived in Appendix A), and the model of Vasyliunas & Siscoe (1976).

The resulting acceleration efficiencies for H, N, O, and Ne are shown in Table 3 and Figure 5 for both the strong and weak shock cases. The acceleration efficiencies are relatively insensitive to the assumed strength of the shock. The results have much smaller uncertainties than in the previous study of Cummings & Stone (1996). Although the new results are consistent with the previous work, the acceleration efficiency for O and Ne are factors of ~ 1.5 and ~ 2.0 larger, respectively, than in the previous work. This is due in part to improved modeling of the modulation process and also due to changes in the estimated neutral abundances at the termination shock reported in the literature. The observed preferential acceleration for the heavier particles is also qualitatively consistent with the results of Gloeckler & Geiss (2001) and qualitatively consistent with Monte Carlo studies of shock acceleration by Ellison, Jones, & Baring (1999), but it is in disagreement with the results of Kucharek & Scholer (1995).

Recently, Zank et al. (2001b) have developed a two-stage acceleration process, each with a mass-dependent efficiency. The first stage involves preacceleration by a multiply reflected-ion (MRI) mechanism that is more efficient for lighter ions and accelerates pickup ions up to ~ 0.5 MeV nucleon^{-1}. This is a sufficiently high energy that the ions can undergo diffusive acceleration to ACR energies. This second stage is more efficient for heavier ions because injection into

TABLE 3
PICKUP ION PARAMETERS AND ACCELERATION EFFICIENCIES RELATIVE TO He

Element	Neutral Density in Outer Heliosphere[a] (cm^{-3})	Total Ionization Rate at 1 AU[b] (10^{-7} s^{-1})	Pickup Ion Flux at Nose of Heliosphere[c] (cm^{-2} s^{-1})	Acceleration Efficiency	
				Strong Shock Case[d]	Weak Shock Case[d]
H	$(9.7 \pm 1.5) \times 10^{-2}$	8.11 ± 1.62	$(1.03 \pm 0.26) \times 10^4$	0.12 ± 0.04	0.15 ± 0.05
He	$(1.6 \pm 0.2) \times 10^{-2}$	1.19 ± 0.24	$(3.06 \pm 0.72) \times 10^2$	1.0	1.0
N	$(7.8 \pm 1.5) \times 10^{-6}$	6.02 ± 1.20	$(6.72 \pm 1.86) \times 10^{-1}$	6.7 ± 2.5	7.1 ± 2.6
O	$(5.3 \pm 0.8) \times 10^{-5}$	8.48 ± 1.70	$(6.13 \pm 1.53) \times 10^0$	5.2 ± 1.8	5.2 ± 1.8
Ne	$(7.6 \pm 1.5) \times 10^{-6}$	3.65 ± 0.73	$(4.18 \pm 1.17) \times 10^{-1}$	4.9 ± 1.8	4.8 ± 1.8

[a] Gloeckler & Geiss 2001.
[b] See Appendix A, except uncertainties are ±20%.
[c] Using model of Vasyliunas & Siscoe 1976.
[d] Defined by eq. (3).

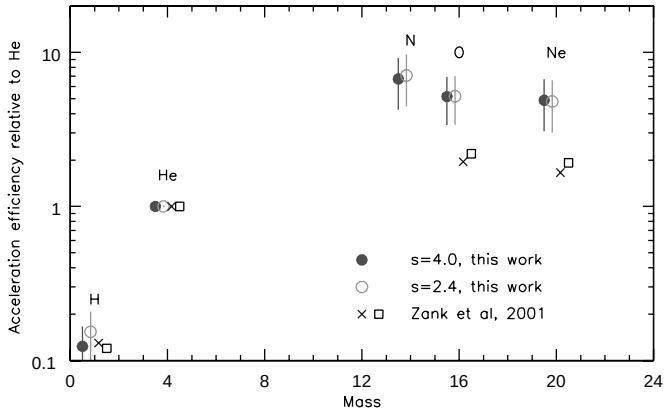

FIG. 5.—Acceleration efficiencies for H^+, N^+, O^+, and Ne^+ relative to He^+ from Table 3. The open circles are for a shock strength of 2.4, and the filled circles are for a shock strength of 4.0. The open squares and crosses are theoretical estimates from Zank et al. 2001b. [*See the electronic edition of the Journal for a color version of this figure.*]

diffusive acceleration occurs at lower energies where the flux of preaccelerated ions is larger. Their model was in reasonable agreement with our earlier estimates. As shown in Figure 5, those calculated values are reasonably consistent with our improved estimates, especially for H. In this model, the strong mass dependence in the efficiency of diffusive acceleration indicates that the scattering near the shock is weak (Zank et al. 2001b).

4.3. *Interstellar* Ar *Abundance*

Interstellar Ar pickup ions have not been measured to date. However, we do have measurements of ACR Ar, and if we assume that the acceleration efficiency for Ar^+ is similar to that of N^+, O^+, and Ne^+, as Figure 5 suggests, we can make an estimate of the neutral Ar density at the solar wind termination shock. The procedure is to use equation (3) to estimate the flux of pickup ion Ar^+ flowing into the nose of the termination shock, and then find the density of neutrals at the shock that would account for that pickup ion flux using the model of Vasyliunas & Siscoe (1976) and the ionization rate of neutral Ar at 1 AU (Appendix A). The result is the ratio of neutral densities, $n_{\rm Ar}/n_{\rm He}$. The local interstellar neutral He density is reasonably well determined by direct measurement to be 0.0155 ± 0.0015 cm^{-3} (Witte, Banaszkiewicz, & Rosenbauer 1996), which agrees well with the value from the pickup ion observations, 0.016 ± 0.002 cm^{-3} (Gloeckler & Geiss 2001). By using the Ar filtration factor derived in Appendix B, we are able to estimate the absolute density of neutral Ar in the VLISM.

The weighted average of the relative acceleration efficiencies for N^+, O^+, and Ne^+ from Table 3 (strong shock case) is 5.4 ± 1.1. The Ar abundance relative to He is taken from Table 2 (strong shock case), and the pickup ion He^+ flux is from Table 3. From equation (3), we find $F_{\rm Ar} = (2.9 \pm 1.1) \times 10^{-2}$ cm^{-2} s^{-1} for the flux of pickup ion Ar^+ flowing into the nose of the termination shock. The ionization rate of interstellar neutral Ar at 1 AU is $(9.91 \pm 1.98) \times 10^{-7}$ s^{-1} (Appendix A), leading to a neutral density of Ar at the termination shock of $(2.2 \pm 0.9) \times 10^{-7}$ cm^{-3}. This density is essentially proportional to the neutral He density (Table 3), so the derived quantity is $n_{\rm Ar}/n_{\rm He} = (1.4 \pm 0.6) \times 10^{-5}$ at the termination shock. This is in agreement within uncertainties of the estimate of $(1.6 \pm 0.5) \times 10^{-5}$ from Gloeckler & Geiss (2001), arrived at by a similar method using an earlier ACR abundance data set (Cummings et al. 1999) and slightly different ionization parameters.

By propagating our density of neutral Ar back through the heliospheric interface, we can compare with models of the ionization state of the VLISM recently computed by Slavin & Frisch (2002). The heliosheath filtration factors are estimated in Appendix B. For Ar, the filtration factor is 0.64 ± 0.11, implying that our estimate of the density of neutral Ar in the VLISM is $(3.5 \pm 1.6) \times 10^{-7}$ cm^{-3}. Slavin & Frisch (2002) computed 25 models of the ionization state of the VLISM, and they featured model 17 as the best-fit model to a variety of observations. Their model 17 value for the neutral Ar density is 1.73×10^{-7} cm^{-3}, about 1.1 σ below our value.

5. LOW-FIP IONS: EVIDENCE FOR A SECOND SOURCE OF ACRs

In addition to the high-FIP ions discussed in the previous section, C, with a FIP of 11.22 eV, has usually been attributed to the interstellar source of ACRs. A turn-up in the C energy spectrum at low energies has been observed in the outer heliosphere for more than 10 yr (Cummings & Stone 1988). Recently, observations of intensity increases at low energies of other low-FIP ions in both the inner and outer heliosphere, such as Mg, Si, and S, have been reported (Reames 1999; Cummings et al. 1999). Such ions with FIPs less than that of H (13.6 eV) are expected to be ionized mostly in the local interstellar medium (Frisch 1998; Slavin & Frisch 2002) and would be almost completely excluded from the heliosphere by the Sun's magnetic field. In addition, some of these elements are expected to be depleted onto dust grains, further diminishing the number of neutrals that could travel into the heliosphere and become ionized and accelerated to ACR energies. Although these low-FIP, low-energy intensity increases in the outer heliosphere may not originate as interstellar neutrals, we will follow common usage in referring to them as ACRs because they are likely accelerated at the termination shock.

Because the low-FIP ions are rare, it is important to make sure that particle identification in the instrument is not compromised by background effects. In Figure 6 we demonstrate that the Low Energy Telescopes of the Cosmic Ray instrument (Stone et al. 1977), which are used in the detection of the low-energy part of the ACR spectra of these ions, contain negligible background for the low-FIP ions of interest: Na, Mg, Si, and S. The two panels show the estimated charge of the ions plotted versus energy: (*a*) is all of the data and (*b*) shows the final selected data set. It is clear that the element groups are well separated and that there is relatively little background.

In Figure 7 we show the energy spectra of these low-FIP ions as observed at *V1* and *V2* over the period 1993/53–1999/365 and at 1 AU (Reames 1999) for the period 1994 November to 1998 April. Also shown are N, O, Ne, and Ar spectra for the same time periods. Most of the energy spectra show turn-ups at low energies, although C at 1 AU may be an exception. The same model transport parameters are used for the calculated spectra for each element (Fig. 3, *left-hand panels*). The ACR intensity level at the shock and the GCR intensity multiplier j_0 (see eq. [2]) are adjusted to fit

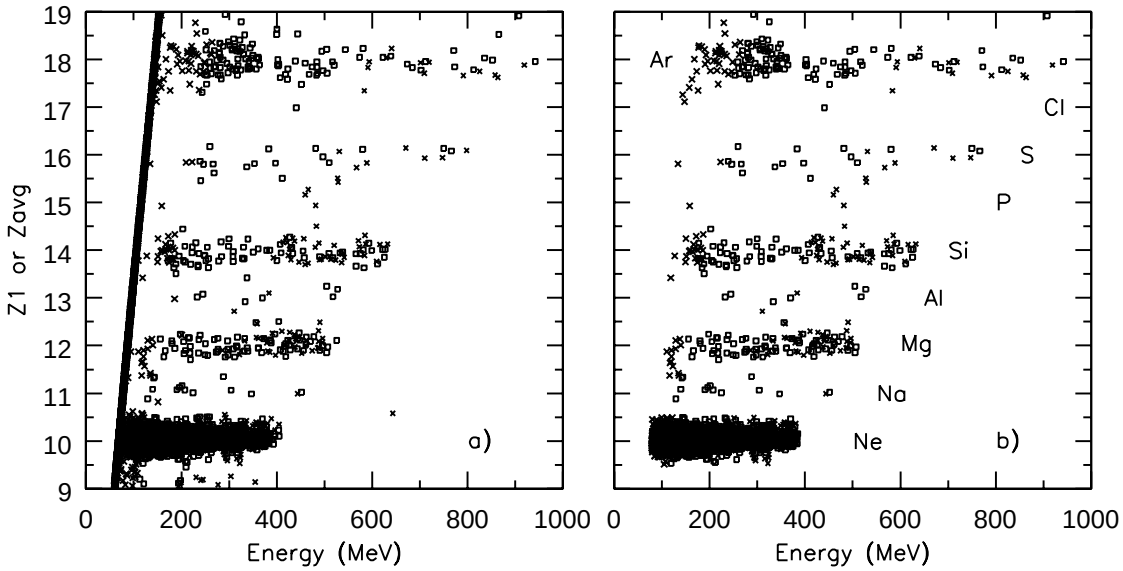

FIG. 6.—(*a*) Nuclear charge vs. energy for particle events in the *V1* LET telescopes collected during 1993/53–1999/365. The crosses (Z1 events) represent the charge estimated when only two of the three detectors registered valid energy depositions. The open squares (Zavg events) represent particles in which three detectors yielded valid measurements. With three parameters, the charge can be estimated in two semi-independent ways. A consistency criterion has been applied for these events. (*b*) Same as (*a*), except selection criteria have been applied to identify particles as being one of Ne, Na, Mg, Si, S, or Ar and having energies in selected energy bins.

the *V1* and *V2* observations. Although the model was not fitted to the spectra at 1 AU, the model spectra for 1 AU are shown for comparison with the observations.

As noted earlier, the longer time interval was chosen to improve the statistical accuracy of the rare elements. All of these elements are observed at higher rigidities where there were limited changes in intensity over this time period. This is confirmed by noting that the best-fit intensities at the shock in Figure 7 for N, O, Ne, and Ar are very similar to those derived for the shorter solar minimum period in Figure 4 (strong shock case). As a result, it is reasonable to use observations over this longer time period to determine the abundances of the low-FIP ions relative to O. As shown in Figure 7, the model fits both the *V1* and *V2* spectra, yielding the relative abundances given in Table 4.

TABLE 4

ABUNDANCES OF ACRs (RELATIVE TO O) AT THE SOLAR WIND TERMINATION SHOCK

Element	Reames[a]	This Work[b]
H	...	$(4.0 \pm 0.2) \times 10^{1}$
He	5.0 ± 0.5	$(9.7 \pm 0.5) \times 10^{0}$
C	$<10^{-2}$	$(4.9 \pm 0.5) \times 10^{-3}$
N	$(1.2 \pm 0.1) \times 10^{-1}$	$(1.4 \pm 0.08) \times 10^{-1}$
O	1.0 ± 0.01	1.0[c]
Ne	$(7.0 \pm 0.7) \times 10^{-2}$	$(6.5 \pm 0.4) \times 10^{-2}$
Na	$<2 \times 10^{-4}$	$(1.6 \pm 0.6) \times 10^{-4}$
Mg	$(1.2 \pm 0.3) \times 10^{-3}$	$(3.7 \pm 1.3) \times 10^{-4}$
Si	$(1.7 \pm 0.3) \times 10^{-3}$	$(1.2 \pm 0.2) \times 10^{-3}$
S	$(6.0 \pm 0.2) \times 10^{-4}$	$(3.9 \pm 1.3) \times 10^{-4}$
Ar	$(4.2 \pm 0.5) \times 10^{-3}$	$(5.0 \pm 0.9) \times 10^{-3}$

[a] Derived from observations at 1 AU (Reames 1999).

[b] H, He, N, Ne, and Ar derived from *V1* and *V2* observations for the period 1998/1–1999/182; all others derived for the period 1993/53–1999/365.

[c] Actual intensity at shock at 0.5 MeV nucleon^{-1} = $(3.71 \pm 0.14) \times 10^{1}$ (m^2 s sr MeV nucleon^{-1})$^{-1}$.

Although the model was not fitted to the 1 AU spectra, it matches the lowest energy intensities (3–5 MeV nucleon^{-1}) of the high-FIP ACRs, N, O, Ne, and Ar. The lowest energy intensities of Mg, Si, and S observed at 1 AU exceed those predicted by the model fits to the *V1* and *V2* spectra, in units of 10^{-4} (m^2 s sr MeV nucleon^{-1})$^{-1}$, by 1.32 ± 0.48, 1.04 ± 0.47, and 0.88 ± 0.30, respectively. It was suggested by Cummings et al. (1999) that these excesses might be evidence for a non-ACR contribution at 1 AU. However, the increases are not consistent with the composition typical of CIR-related events owing to the absence of a corresponding increase in the Fe flux (Reames 1999).

Assuming that the 1 AU intensities of Mg, Si, and S are due to ACRs accelerated at the termination shock leads to estimates for the relative abundances of these species at the termination shock (Reames 1999) that are larger than determined from the *V1* and *V2* spectra, as shown in Table 4. In contrast, with the exception of Ne, estimates of the abundances at the shock of high-FIP ions based on 1 AU data are lower than from the *Voyager* data acquired between 39 and 79 AU. This may reflect the greater solar modulation of the 1 AU intensities and the correspondingly larger uncertainties in the demodulated spectrum at the termination shock.

6. SOURCES OF THE LOWER FIP ACRs IN THE OUTER HELIOSPHERE

We consider five possible sources for the low-energy turnups in the energy spectra of C, Na, Mg, Si, and S at *V1* and *V2* shown in Figure 7: a low-energy CIR component, solar wind ions, interstellar neutrals, interstellar singly charged ions, and the recently discovered "inner" source of pickup ions.

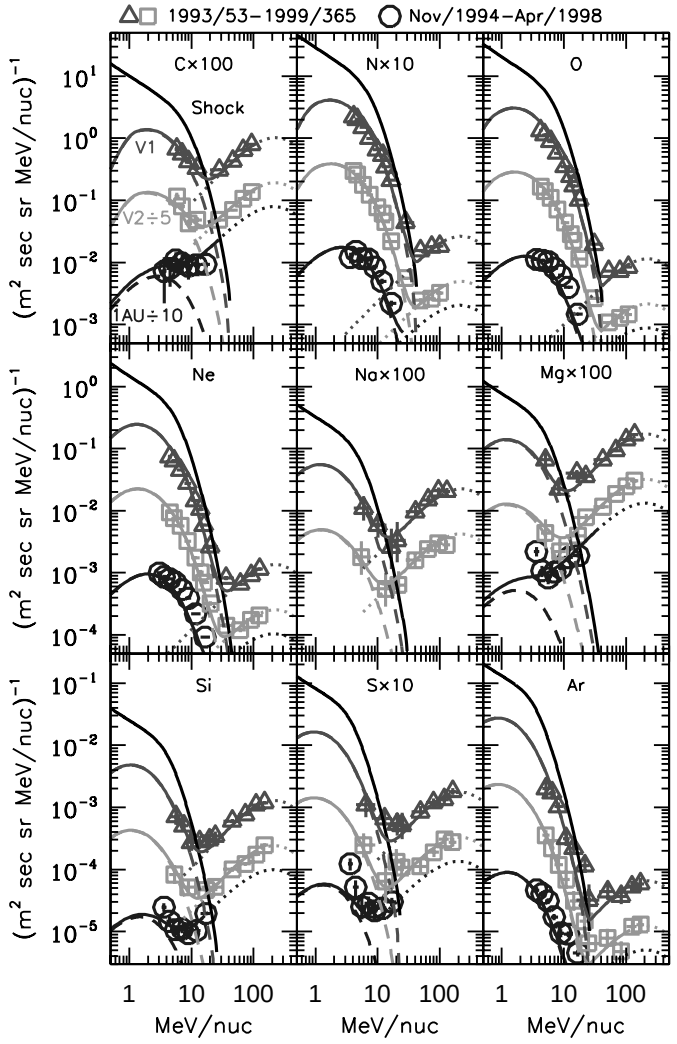

FIG. 7.—Same as left-hand of panels of Fig. 4 except that data and calculations are for C, N, O, Ne, Na, Mg, Si, S, and Ar and the time period is 1993/53–1999/365 for the *V1* and *V2* data. Also shown are energy spectra from Reames (1999) at 1 AU (*open circles*) for the period 1994 November–1998 April. Some data are scaled as in Fig. 4 for clarity purposes. In the case of 1 AU spectra, the same factor as for *V1* is used plus an additional factor of 0.1. The fits are to the *V1* and *V2* data only as in Fig. 4. The shock is assumed to be strong, $s = 4$. [*See the electronic edition of the Journal for a color version of this figure*.]

6.1. *Possible CIR Component in the Outer Heliosphere*

There is a CIR enhancement in the *V1* and *V2* energy spectra of protons. We scale the *V2* H CIR component, which is better defined than that present in the *V1* H spectrum, to the other elements using relative abundances from Table 2 of Richardson et al. (1993) for solar minimum corotating events. In Figure 8 we show the observed *V2* energy spectra of H, C, Mg, Si, and S, along with the estimated CIR spectra. The estimated CIR intensities are factors of 1/40 to 1/400 that of the observations at the lowest energy, strongly suggesting that the low-energy turnups in the spectra of C, Mg, Na, Si, and S at *V1* and *V2* are not due to a local CIR component.

6.2. *Solar Wind Ions as a Source*

A possible source of the low-FIP ACRs is the injection and acceleration at the termination shock of a small fraction

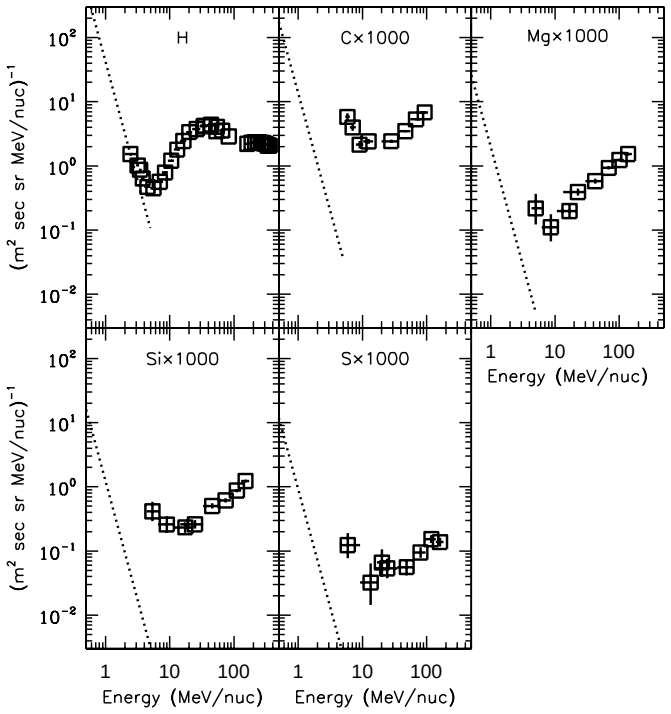

FIG. 8.—Energy spectra at *V2* of H, C, Mg, Si, and S for the time period 1993/53–1999/365. Also shown are estimated CIR spectra as described in the text.

of the solar wind (Mewaldt 1999). Because the solar wind ions are highly ionized, their acceleration and propagation and the resulting spectra will differ from the model calculations in Figure 7 for singly ionized species. The calculated energy spectra in Figure 9 at *V1* and *V2* are for injected ions of ACR C, Na, Mg, Si, and S with charge states typical of the solar wind (Mewaldt 1999 for C, Mg, Si, and S and Arnaud & Rothenflug 1985 for Na at a temperature of $10^{6.1}$ K). The best fits to the sum of the GCR and ACR contributions are shown. With the exception of the *V1* S spectrum, the observations are not well matched by the model. For most of the ions, the peak energy of the calculated ACR energy spectra occurs at too high an energy to match the observations, falling near where the observed intensity is a minimum.

To quantify the difference between fits with $Q = 1$ and high Q, we compare the χ^2 for the low-energy data points representing the turnup in the energy spectra of Figures 7 and 9. Specifically, for *V1*, we consider the lowest four points for C, the lowest two for Na, the lowest one for Mg, the lowest three for Si, and the lowest two for S. For *V2*, we use the lowest four points for C, the lowest point for Na, the lowest one for Mg, the lowest two for Si, and the lowest one for S. This totals 21 points. For the purposes of this comparison we omit the 15% systematic uncertainties on the data points that were included when the fits were made. The χ^2 for the singly charged case (Fig. 7) is 27.4 and that for the solar wind charge-state case (Fig. 9) is 249.2. Whereas the model is reasonably consistent with the data for the singly charged case (reduced $\chi^2 = 1.3$), it is inconsistent with the solar wind charge-state case (reduced $\chi^2 = 11.9$). The eight carbon points account for ~80% of the χ^2 in both cases. If C is omitted in the calculation of χ^2, the model fits favor the singly charged case (reduced χ^2 of 0.5 vs. 2.7 for the solar

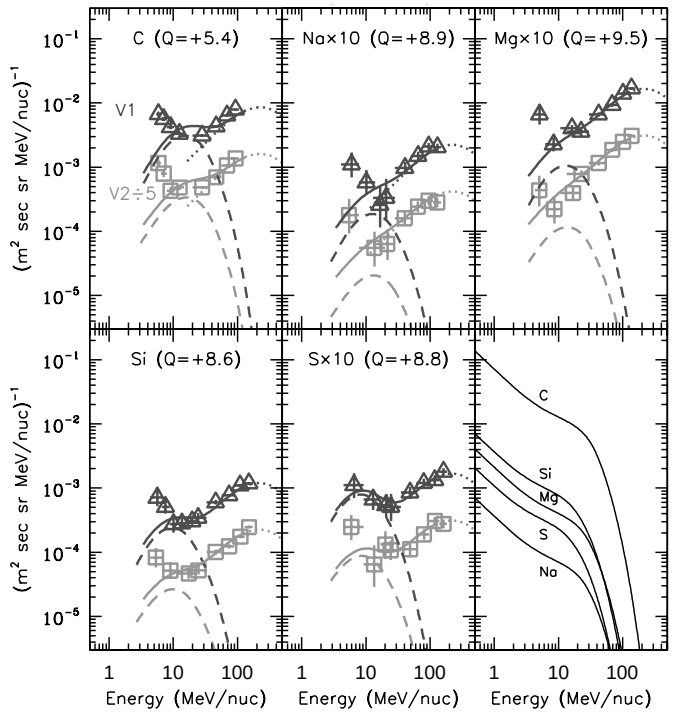

FIG. 9.—Points are the energy spectra of C, Na, Mg, Si, and S at *V1* and *V2* from Fig. 7. The dashed lines are model ACR spectra using the same parameters as used in Fig. 7 except that the charge states of the seed particles are the charge states typical of the solar wind (Mewaldt 1999; Arnaud & Rothenflug 1985). The solid curves are the sum of the ACR (*dashed*) and GCR (*dotted*) curves. The 1 AU data and curves have been omitted for clarity. The lower right-hand panel shows the calculated energy spectra at the solar wind termination shock at 90 AU at a polar angle of 30°. [*See the electronic edition of the Journal for a color version of this figure.*]

wind charge-state case). We conclude that it is unlikely that accelerated solar wind ions account for the energy spectra of the elements of Figure 9 at low energies.

Since the source for C, Mg, Si, and S is unlikely to be the solar wind, spectra at the shock in Figure 9 associated with these fits represent upper limits to the acceleration of these solar wind ions by the termination shock. With these upper limits to the intensities at the shock at 0.5 MeV nucleon^{-1} and estimates of the solar wind fluxes at 90 AU, equation (3) can be used to determine an upper limit to the acceleration efficiencies for these ions relative to interstellar pickup He. The solar wind fluxes are scaled from the 1 AU solar wind proton flux of 2.5×10^8 cm^{-2} s^{-1} (Schwadron & Geiss 2000) using the elemental abundances in the fast solar wind (von Steiger et al. 2000). We find $\epsilon_{SW,C} \leq 1 \times 10^{-2}$, $\epsilon_{SW,Mg} \leq 2 \times 10^{-3}$, $\epsilon_{SW,Si} \leq 4 \times 10^{-3}$, and $\epsilon_{SW,S} \leq 2 \times 10^{-3}$. Thus the acceleration efficiencies for highly charged ions are typically less than 10^{-3} of the acceleration efficiencies for singly charged N, O, and Ne shown in Table 3.

6.3. *Interstellar Neutrals as a Source*

Based on the comparison of earlier compilations of interstellar and ACR abundances, Mewaldt (1999) concluded that the abundances of interstellar neutral Si, S, and Fe were less than a tenth of that required to account for the ACRs. We have revisited that analysis using recent calculations by Slavin & Frisch (2002) of 15 neutral elemental gases in the local interstellar medium (LISM), including all those of interest in this study. They model the ionizing radiation field within ~5 pc of the Sun and carry out radiative transfer calculations to estimate the ionization state abundances of the gases. They use 25 different sets of input parameters to generate 25 models of the abundances. We compare our ACR abundances with their best-fit model 17.

In order to estimate the expected contribution of these low-FIP neutrals to the ACR observations, we will calculate the flux of pickup ions at the nose of the heliosphere and compare with the pickup ion flux required to account for the ACR intensities inferred at the shock. For the latter, we use the values in Table 3 for H, He, N, O, and Ne. For Ar, we use the value derived in § 4.3. For C, Na, Mg, Si, and S, we derive the pickup ion flux using the same method as used for Ar and the ACR intensities at 0.5 MeV nucleon^{-1} from Figure 7. For the ions where we have no direct acceleration efficiency determination, we use the average of the N, O, and Ne acceleration efficiencies as we did for Ar in § 4.3. These pickup ion fluxes are shown in Figure 10 as the filled circles (based on Gloeckler & Geiss 2001) and filled diamonds (based on ACR observations and the strong shock acceleration efficiencies of Table 3).

To estimate the pickup ion fluxes implied by the calculated neutral densities from Slavin & Frisch (2002), we require knowledge of the filtration factor in the heliosheath and beyond for each neutral atom, defined as the ratio of the neutral density just inside the solar wind termination shock to that in the unperturbed interstellar medium. These factors are estimated in Appendix B. Using these factors,

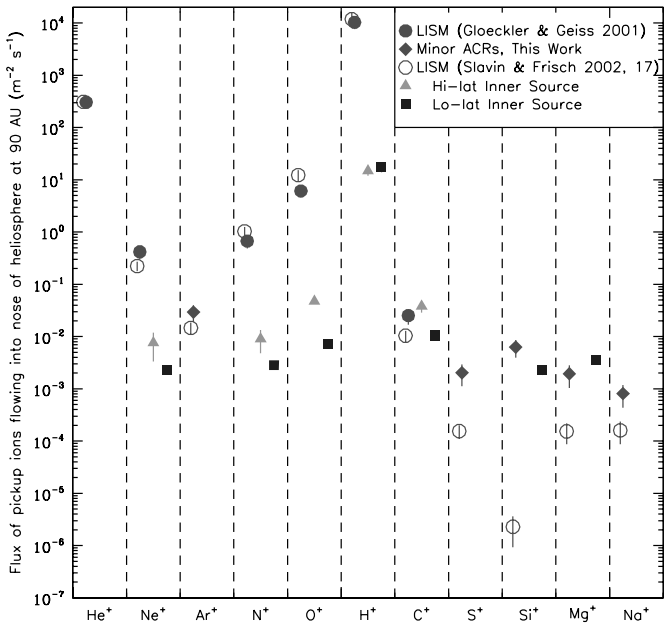

FIG. 10.—Estimated flux of interstellar and inner source pickup ions flowing into the nose of the heliosphere at 90 AU, the assumed location of the solar wind termination shock. The ions are arranged from left to right in descending order of first ionization potential. The solid circles are estimated from neutral densities in the outer heliosphere from Gloeckler & Geiss (2001), ionization rates at 1 AU from Table 7, and the theory of Vasyliunas & Siscoe (1976). The open circles are derived from the neutral densities in the local interstellar medium from model 17 of Slavin & Frisch (2002), the filtration factors of Appendix B, the ionization rates at 1 AU from Table 7, and the theory of Vasyliunas & Siscoe (1976). The filled diamonds are based on the inferred intensities of ACRs at the shock at 0.5 MeV nucleon^{-1} and the average of the acceleration efficiencies of N^+, O^+, and Ne^+ are from Table 3 (strong shock case), which are shown in Fig. 5. [*See the electronic edition of the Journal for a color version of this figure.*]

the neutral densities in the LISM from model 17 of Slavin & Frisch (2002), and the ionization rate of the neutrals at 1 AU (Appendix A), we derive the interstellar pickup ion fluxes shown in Figure 10.

In general, there is reasonable agreement (factor of ~2–3) between the pickup ion fluxes inferred from the Slavin & Frisch (2002) calculations and those inferred from the pickup ion/ACR observations for all the high-FIP elements H, He, N, O, Ne, and Ar, as well as for the low-FIP element C.

For Na, Mg, Si, and S, however, the interstellar neutral pickup ion fluxes are well below the values indicated from the ACR observations. The interstellar pickup ion fluxes of Na, Mg, Si, and S in Figure 10, based on estimates of model 17 of Slavin & Frisch (2002), are factors of 5.0, 12.7, 2736, and 13.1, respectively, below those inferred from the ACR observations. Thus, to account for Na, Mg, Si, and S ACRs, the acceleration efficiencies for interstellar pickup Na^+, Mg^+, Si^+, and S^+ would have to be 5.0, 12.7, 2736, and 13.1, respectively, times that shown in Figure 5 for N^+, O^+, and Ne^+. This seems unlikely.

6.4. *Interstellar Singly Charged Ions as a Source*

According to the models of Slavin & Frisch (2002), most of the low-FIP ions of interest to this study are in the singly ionized state in the VLISM. From the study of filtration by Izmodenov, Lallement, & Geiss (1999), a small fraction of H^+ and O^+ is neutralized in the heliosheath and maintain trajectories that allow some of these secondary neutrals to enter the heliosphere. So it is reasonable to ask whether such a neutralization process and subsequent ionization and acceleration at the termination shock could account for the low-FIP ACR intensities of C, Na, Mg, Si, and S. In Appendix B we calculate the fraction of primary interstellar neutral atoms that reach the termination shock after traversing the heliosheath and suffering losses as a result of photoionization, electron-impact ionization, and charge exchange with H^+. The trajectories of these neutrals are not affected by magnetic fields, so we use a simple exponential attenuation calculation using the appropriate interaction cross sections and rate coefficients. Singly charged ions in the VLISM, however, will be deflected around the heliosphere for the most part by the heliospheric magnetic field, particularly between the bow shock and the heliopause and between the heliopause and the termination shock (see, e.g., Zank, Müller, & Wood 2001a). When they interact with the neutral H through charge exchange or become neutralized by radiative or dielectronic recombination with electrons in these regions, the trajectories of the newborn neutrals will be the same as those of the singly charged parent ion and hence not generally toward the inner heliosphere. To model this phenomenon accurately, a Monte Carlo approach, as was done for the filtration of H and O by Izmodenov et al. (1999), would be required. In this work we choose to estimate the maximum possible contribution from this source by assuming that the trajectories of the singly charged ions are not affected by the heliospheric magnetic field and use a simple exponential attenuation formula to estimate the upper limit to the density of secondary neutrals that reach the termination shock. This secondary density can be compared to the estimated primary interstellar neutral density at the termination shock.

To accomplish this, we consider C^+ and S^+, the two singly charged low-FIP ions for which we could find all three required rate coefficients: for charge-exchange with neutral H, for radiative recombination with electrons, and for dielectronic recombination with electrons. These rate coefficients are given in Table 5 for the plasma properties relevant to this study.

The maximum fraction of singly charged ions that are incident on the heliosphere and that are converted to neutrals by the time they reach the termination shock is given by

$$M = 1 - \exp\left[-\frac{1}{v_b}\int_{r_1}^{r_2}(\alpha_{\rm rec} n_e + \alpha_{\rm ce} n_{\rm H})dx\right], \qquad (4)$$

where v_b is the bulk flow velocity, r_1 is 475 AU (assumed to be the start of unperturbed VLISM), r_2 is 90 AU (assumed location of the termination shock), $\alpha_{\rm rec}$ is the temperature-dependent rate coefficient for the sum of radiative and dielectronic recombination, n_e is the electron density, $\alpha_{\rm ce}$ is the rate coefficient for charge exchange with neutral H, and $n_{\rm H}$ is the neutral H density. The integration is performed in a piecewise fashion over the three regions of the heliosphere between the VLISM and the termination shock, as described in Appendix B. In addition to the plasma parameters listed in Appendix B for the three regions, we assume that the temperature of neutral H is 8000 K and the density of neutral H is 0.2 cm^{-3} beyond the heliospheric bow shock and 0.4 cm^{-3} inside the bow shock. We find that the factor M, the maximum fraction of singly charged ions in the VLISM converted to neutrals at the termination shock, is 8.6×10^{-5} for C and 8.4×10^{-5} for S.

Using these factors, the filtration factors for primary interstellar neutral C and S from Appendix B, and the ratios of interstellar C^+/C^0 and S^+/S^0 from model 17 of Slavin & Frisch (2002) (1862 and 7878, respectively [J. Slavin 2001, private communication]), we find that the ratios of secondary to primary neutrals at the termination shock are $C_{\rm sec}/C_{\rm prim} = 0.24$ and $S_{\rm sec}/S_{\rm prim} = 1.34$. Examining Figure

TABLE 5

Rate Coefficients in $cm^3\ s^{-1}$ for Radiative and Dielectronic Recombination with Electrons and Charge Exchange with Neutral H for C^+ and S^+

	Radiative Recombination[a]			Dielectronic Recombination[b]			Charge Exchange[c]
Ion	8000 K	20,000 K	1.5×10^6 K	8000 K	20,000 K	1.5×10^6 K	(8000 K)
C^+.....	5.40×10^{-13}	3.05×10^{-13}	2.06×10^{-14}	1.06×10^{-14}	1.06×10^{-14}	7.93×10^{-13}	2.60×10^{-17}
S^+	4.72×10^{-13}	2.65×10^{-13}	1.75×10^{-15}	9.14×10^{-19}	9.14×10^{-19}	8.30×10^{-13}	1.41×10^{-14}

[a] Aldrovandi & Péquignot 1973.
[b] Mazzotta et al. 1998.
[c] Kingdon & Ferland 1996.

10, the interstellar pickup ion fluxes of C and S are factors of $\gtrsim 2$ and $\gtrsim 5.6$ below those inferred from the ACR observations. While ACR C may well contain a significant contribution from interstellar atoms and ions, it appears that there is still a significant deficit of interstellar S to account for the ACR S observations.

Although we did not find charge-exchange rate coefficients for Na^+, Mg^+, and Si^+ on neutral H, the radiative and dielectronic recombination rate coefficients are similar in magnitude to the same rates for S. For Si, in particular, where the interstellar primary neutral abundance is a factor of 2736 too low to explain the ACR observations, it is very unlikely that enough interstellar singly charged Si can be neutralized and appear in the heliosphere to account for the ACR Si observations. Although a proper Monte Carlo calculation should be carried out, it appears that interstellar singly charged ions likely make a significant contribution only to ACR H and ACR O.

6.5. *Inner Source of Pickup Ions as a Source*

Recently, an "inner source" of singly charged ions has been discovered (Geiss et al. 1995; Schwadron et al. 1999; Gloeckler et al. 2000a, 2000b). These may arise if a solar wind ion impinges on an interplanetary dust grain whose surface is already saturated with solar wind ions that have been neutralized after they were embedded in the dust grain (Fahr, Ripken, & Lay 1981). As the new ion strikes the surface, a neutral solar wind atom is ejected and soon becomes ionized in the same way that an interstellar neutral atom would, through photoionization or charge exchange with the solar wind. Most of these dust grains are in orbits very close to the Sun, within $\sim$10 to $\sim$50 solar radii (Schwadron et al. 2000). The pickup ions cool significantly by the time they reach several AU and so do not have the same velocity distributions in the solar wind rest frame that the interstellar pickup ions do. The detection of Ne in this component with approximately the solar abundance was the crucial diagnostic for the origin of the inner source, as Ne would not be expected to be present in the bulk material of the grain. Hence it is not likely that vaporization or disintegration of the grain itself is the origin of the particles.

We can estimate the flux of inner source ions flowing into the solar wind termination shock in two different latitude regimes from observations reported in Gloeckler et al. (2000a, 2000b), Schwadron et al. (1999), and N. A. Schwadron and G. Gloeckler (2000, private communication). For the low-latitude case, Gloeckler et al. (2000b) estimate the radial distribution at low latitudes of the density of inner source O. From their Figure 7, we estimate that at 1 AU, the density of inner source O^+ is 1.45×10^{-6} cm^{-3} and falling off with radius as $1/r^2$ for $r > 1$ AU. Using a typical solar wind velocity of 400 km s^{-1}, we find that the flux of inner source O^+ at the termination shock at 90 AU is 7.2×10^{-3} cm^{-2} s^{-1}. The low-latitude fluxes of inner source H^+, C^+, N^+, Ne^+, Mg^+, and Si^+ can be derived from abundances relative to O^+ given in Gloeckler et al. (2000a).

At high latitudes, during solar minimum, Schwadron et al. (1999) find the density of inner source O^+ to be 5.5×10^{-7} cm^{-3} at 3 AU. The solar wind speed was observed to be 780 km s^{-1}, which implies a flux of O^+ pickup ions at 90 AU $= 4.8 \times 10^{-2}$ cm^{-2} s^{-1}. The corresponding fluxes of inner source H^+, C^+, N^+, and Ne^+ can be derived from the abundances relative to O^+ in N. A. Schwadron and G. Gloeckler (2000, private communication). The low- and high-latitude inner source pickup ion fluxes at the solar wind termination shock at 90 AU are shown in Figure 10.

As shown in the figure, the inner source pickup ion fluxes of C, Mg, and Si are comparable to those inferred from the ACR observations, which were based on the same relative acceleration efficiency as for the interstellar source. Thus if the inner source were to explain the ACR observations of C, Mg, and Si, the acceleration efficiency would need to be approximately the same as for the interstellar pickup ions. Given the differences in the velocity distributions of inner source and interstellar pickup ions, it is not obvious that this should be so. Note that it is unlikely that the inner source can account for the high-FIP ACRs (H, N, O, and Ne) because the acceleration efficiency would have to be 10–1000 times higher for inner source H, N, O, and Ne than for C, Mg, and Si.

6.6. *Discussion*

Interstellar pickup ions accelerated by the termination shock of the solar wind are the principal component of anomalous cosmic rays. By comparing the intensities of ACR H, He, N, O, and Ne with estimates of the pickup ion flux at the shock, relative acceleration efficiencies have been derived for diffusive shock acceleration. Combining these acceleration efficiencies with observations of ACR Ar, it is possible to infer the flux of Ar^+ pickup ions flowing into the solar wind termination shock. Using the model of Vasyliunas & Siscoe (1976) and the ionization rates at 1 AU of neutral Ar, we have inferred the neutral density of Ar at the location of the termination shock. Applying a filtration factor for losses of neutral Ar and of neutral H, He, N, O, and Ne from Gloeckler & Geiss (2001) in traversing the heliospheric interface, we have derived estimates for the neutral densities of H, He, N, O, Ne, and Ar in the VLISM.

Slavin & Frisch (2002) have developed a series of models of the local interstellar medium based on different sets of parameters. As shown in Figure 11, the neutral densities derived from pickup ions (Gloeckler & Geiss 2001) and from ACRs generally agree with their favored models 17 and 18 to within a factor of $\sim$2 for densities from $\sim 10^{-1}$ to $\sim 10^{-5}$ cm^{-3}.

We note that although ACR C requires more interstellar neutrals than in models 17 and 18 (see Fig. 10), it is also possible that some of the ACR C arises from a second source that is also the source of the ACR Na, Mg, Si, and S. This will be difficult to assess without a better understanding of the origin of the second source discussed below.

Because the *Voyager 1* and *2* spacecraft were likely within $\sim$20 and $\sim$35 AU, respectively, of the termination shock during a period of minimum modulation, ACR Na, Mg, Si, and S, which have relatively small abundances, are observable. However, these elements are apparently not interstellar in origin because their interstellar neutral densities are much too small. While a small fraction of interstellar singly charged ions are neutralized in the heliosheath, it appears that the relatively small cross sections for the neutralization processes and the deflected trajectories of these particles make it unlikely that they contribute significantly to the ACR observations. Thus, there is evidence for another source of ACR ions other than interstellar atoms.

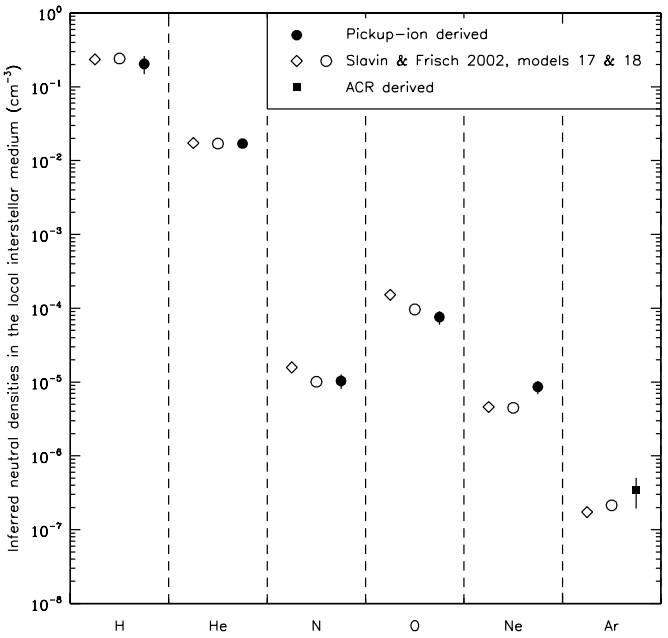

FIG. 11.—Estimated neutral densities of six atoms in the VLISM. The pickup-ion–derived values are based on estimates of the neutral densities at the termination shock from Gloeckler & Geiss (2001) and the filtration factors from Appendix B. (See Table 10.)

The spectral shapes of ACR Mg and Si are consistent with singly charged Mg and Si and peak at much lower energies than would be the case for multiply charged ions accelerated from the solar wind. The abundances of the low-energy spectral increases relative to H also differ significantly from that of particles accelerated by corotating interaction regions. Thus, neither the solar wind nor CIRs are a likely source, and the acceleration efficiencies for solar wind ions such as $Mg^{+9.5}$, $Si^{+8.6}$, and $S^{+8.8}$ are less than 10^{-3} of that for N^+, O^+, and Ne^+.

The recently discovered inner source of pickup ions appears to be a possible source of these rarer ACRs. For that to be the case, however, the acceleration efficiency for inner source and interstellar pickup ions would have to be similar, even though their velocity distributions in the solar wind are much different. Assessing the likelihood of this requires an improved understanding of the acceleration process and the possible role of the ubiquitous suprathermal tails recently observed in both solar wind and pickup ion velocity distributions (Gloeckler et al. 2000b; Fisk et al. 2000).

We thank E. Christian for algorithms to analyze the H and He events that do not stop within the CRS detectors (e.g., $\gtrsim$80 MeV nucleon^{-1}). We thank D. Reames for providing machine-readable intensities for the 1 AU *Wind* energy spectra. We thank the MIT Space Plasma Group for making *IMP 8* data available at their website (ftp://space.mit.edu/pub/plasma/imp/www/imp.html). SOLAR2000 Research Grade historical irradiances are provided courtesy of W. Kent Tobiska and SpaceWx.com. These historical irradiances have been developed with funding from the NASA *UARS*, *TIMED*, and *SOHO* missions. We appreciate valuable discussions with R. Leske, A. F. Barghouty, N. Schwadron, G. Gloeckler, J. Slavin, P. Frisch, K. Tobiska, G. Ferland, F. Keenan, and P. Stancil. This work was supported by NASA under contract NAS 7-1407.

APPENDIX A

IONIZATION RATES IN THE INTERPLANETARY MEDIUM

The ionization processes in the interplanetary medium that govern the flux of pickup ions flowing into the solar wind termination shock are due primarily to photoionization by solar photons and charge exchange with solar wind protons (Rucinski et al. 1996). We follow the general methods used by Rucinski et al. (1996) in calculating the ionization rates of H, He, C, N (photoionization only), O, Ne, and Ar at 1 AU. We extend the calculations to all 11 elements involved in this study: H, He, C, N, O, Ne, Na, Mg, Si, S, and Ar.

For the charge-exchange reaction $X + H^+ \rightarrow X^+ + H$, we use daily solar wind speed and proton flux data from *IMP 8* and cross sections from various sources to compute the daily ionization rates for the period 1978–1998. We form the yearly averaged ionization rates from the daily values and then compute the average ionization rate from the 21 yearly averaged values.

The references for the cross sections are given in Table 6. We note that relatively little data and/or calculations exist for charge exchange with protons in the energy range of interest for N, Si, and S. The method used by Kimura et al. (1997a) for O appears to produce cross sections that are too large by a factor of $\sim$2.9 when compared to the data of Stebbings, Smith, & Ehrhardt (1964). The latter data are in good agreement with the recommended cross sections from Stancil et al. (1999). Therefore, for S and Si we scale the cross section for S in Kimura et al. (1997a) and for Si in Kimura et al. (1996) by the factor 1/2.9. The cross section for N in Kimura et al. (1997a) does not extend in energy as far as we require. Over the energy range of interest below the maximum energy at which they make their calculation (1 keV nucleon^{-1}), the N/O cross section ratio is $\sim$1/2.9. Therefore, we assume that the cross section for N relative to O in Kimura et al. (1997a) is correct and use the cross section for O given in Stancil et al. (1999) divided by 2.9 to represent that of N. The cross sections are shown as a function of solar wind velocity in Figure 12.

The resulting charge-exchange ionization rates are given in Table 7. The major differences from Rucinski et al. (1996) are the use of different cross sections for some elements and the different run of 21 yr; we started in 1978 and Rucinski et al. (1996) started in 1974.

Our photoionization calculations differ somewhat from the method of Rucinski et al. (1996), who used only two solar irradiance spectra, one to represent solar maximum and one to represent solar minimum, and then scaled the entire spectrum by a linear function of the F10.7 parameter to get the estimated spectrum for each year. Rucinski et al. (1996) used cross sections from a variety of sources. In the present work we use analytic representations of the cross sections from Verner et al. (1996)

TABLE 6
REFERENCES FOR CHARGE-EXCHANGE CROSS SECTIONS WITH SOLAR WIND H^+

Element	Reference
H	Barnett et al. 1990, pp. A22–A23[a]
He	Barnett et al. 1990, pp. A32–A33[a]
C	Stancil et al. 1998[a]
N	Kimura et al. 1997a[a,b]
O	Stancil et al. 1999[a]
Ne	Nakai et al. 1987[c]
Na	Tabata et al. 1988[c]
Mg	Tabata et al. 1988[c]
Si	Kimura et al. 1996[a,d]
S	Kimura et al. 1997b[a,d]
Ar	Nakai et al. 1987[c]

[a] Approximated with power-law segments in keV nucleon^{-1}.
[b] Assumed cross section is that of O in Stancil et al. 1999 divided by 2.9 based on calculated values for both elements near 1 keV in this reference.
[c] Used analytic function provided in reference.
[d] Summed partial cross sections from ground state to final states and divided by 2.9.

and new solar irradiance spectra available on a daily basis from the SOLAR2000RG model (Tobiska et al. 2000). We use the 1 nm output from the SOLAR2000RG model (Version 1.20a).[1] We compute daily estimated solar spectra in units of photons cm^{-2} s^{-1} in 1 nm bins from 0.5 to 242 nm. We then convolve the yearly spectra with the cross sections to produce yearly averaged ionization rates for each of the 11 elements. The calculated average photoionization rates for the 21 yr are given in Table 7.

[1] Available at http://www.spacewx.com.

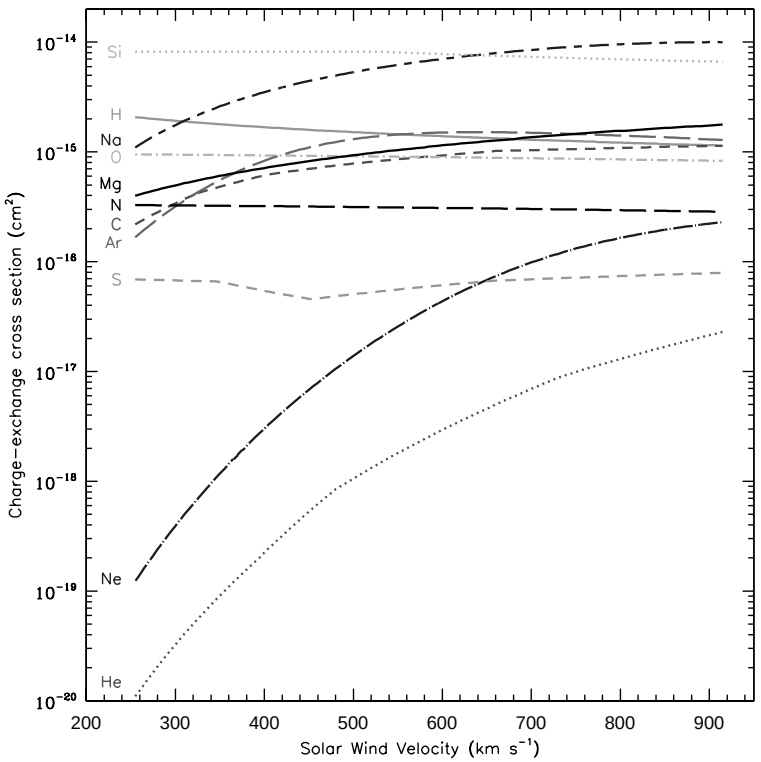

FIG. 12.—Charge-exchange cross sections from the references in Table 6 vs. solar wind velocity. The range of velocities shown represents the range of daily values from *IMP 8* over the years 1978–1998. [*See the electronic edition of the Journal for a color version of this figure.*]

TABLE 7
IONIZATION RATES AT 1 AU

Element	Charge-Exchange Ionization Rate[a] (s^{-1})	Photoionization Rate[a] (s^{-1})	Total Ionization Rate[a] (s^{-1})
H	$(6.44 \pm 0.14) \times 10^{-7}$	$(1.67 \pm 0.05) \times 10^{-7}$	$(8.11 \pm 0.13) \times 10^{-7}$
He	$(3.40 \pm 0.39) \times 10^{-10}$	$(1.18 \pm 0.10) \times 10^{-7}$	$(1.19 \pm 0.10) \times 10^{-7}$
C	$(2.51 \pm 0.08) \times 10^{-7}$	$(1.44 \pm 0.07) \times 10^{-6}$	$(1.69 \pm 0.07) \times 10^{-6}$
N	$(1.25 \pm 0.03) \times 10^{-7}$	$(4.77 \pm 0.26) \times 10^{-7}$	$(6.02 \pm 0.26) \times 10^{-7}$
O	$(3.61 \pm 0.08) \times 10^{-7}$	$(4.86 \pm 0.30) \times 10^{-7}$	$(8.48 \pm 0.30) \times 10^{-7}$
Ne	$(4.67 \pm 0.53) \times 10^{-9}$	$(3.60 \pm 0.29) \times 10^{-7}$	$(3.65 \pm 0.29) \times 10^{-7}$
Na	$(1.57 \pm 0.06) \times 10^{-6}$	$(5.37 \pm 0.00) \times 10^{-6}$	$(6.95 \pm 0.07) \times 10^{-6}$
Mg	$(3.06 \pm 0.10) \times 10^{-7}$	$(5.42 \pm 0.08) \times 10^{-7}$	$(8.48 \pm 0.14) \times 10^{-7}$
Si	$(3.17 \pm 0.07) \times 10^{-6}$	$(2.77 \pm 0.07) \times 10^{-5}$	$(3.09 \pm 0.07) \times 10^{-5}$
S	$(2.25 \pm 0.05) \times 10^{-8}$	$(3.45 \pm 0.16) \times 10^{-6}$	$(3.48 \pm 0.16) \times 10^{-6}$
Ar	$(3.57 \pm 0.14) \times 10^{-7}$	$(6.34 \pm 0.31) \times 10^{-7}$	$(9.91 \pm 0.35) \times 10^{-7}$

[a] Uncertainties shown are derived from standard deviation of 21 yearly averaged values. Actual uncertainties used in analysis are ±20%.

The sum of the photoionization and charge-exchange ionization rates are also given in Table 7. In Rucinski et al. (1996), the uncertainties on the computed rates were estimated by dividing the standard deviation of the 21 yearly values for each element by $\sqrt{21}$.

We show the same type of uncertainties in Table 7; however, we feel these are somewhat too small. Photoionization dominates the ionization rate for all elements except H. While the photoionization cross sections are accurate to perhaps 10%–20% (see, e.g., Nahar, Pradhan, & Zhang 2001), the solar UV flux below 105 nm is relatively uncertain, with uncertainties of 90% to factors of 4 for some wavelengths (see 809 wavelength output of SOLAR2000RG model). At higher wavelengths, above 150 nm, the uncertainties are much reduced to ~10% (Woods et al. 1996). The large uncertainties at short wavelengths affect primarily the high-FIP atoms, H, He, N, O, Ne, and Ar. However, pickup ion velocity distributions measured by Gloeckler & Geiss (2001) provide an independent estimate of the total ionization rate, and our estimates are within ~20% of their values, except for H, where we differ by 47%. Accordingly, we adopt an uncertainty of ±20% for the total ionization rates in this work.

APPENDIX B

FILTRATION IN THE HELIOSPHERIC INTERFACE

The ratio of the neutral density of an atomic species just inside the solar wind termination shock to the same density in the unperturbed VLISM is defined as the filtration factor for that atom. Filtration factors for H and O in a two-shock model of the heliosphere have been calculated by Izmodenov et al. (1999). They included the effects of electron-impact ionization, photoionization, charge exchange with H^+, and its reverse process, charge-exchange recombination with neutral H, using a Monte Carlo method. They find, for the set of plasma properties they assumed, that the estimated filtration factors for H and O are 0.475 and 0.7, respectively. These values are in reasonable agreement with those used by Gloeckler & Geiss (2001) for H and O, 0.54 ± 0.05 and 0.62 ± 0.06, respectively, based on an entirely different approach. In the case of these two atoms, the reverse charge-exchange recombination process with neutral H has a significant cross section at low interaction energies, leading to a significant fraction of neutral atoms in the heliosphere that originate as singly charged atoms in the VLISM. In § 6.4 we addressed the issue of singly charged ions of C and S in the VLISM becoming neutralized in the heliosheath and entering the heliosphere. For these two ions, the maximum contribution is not large. We have also compared the charge-exchange rate coefficient of N^+ on neutral H with that of O^+ on neutral H and find it is about a factor of 1000 smaller. The radiative and dielectronic recombination rates are similar but much smaller than the O^+ charge-exchange rate coefficient with neutral H. Thus we do not expect that interstellar singly charged ions will make a significant contribution to the neutral density of atoms at the termination shock, except for interstellar H^+ and O^+. Therefore for He, C, N, Ne, Mg, Si, S, and Ar, we consider only the filtration of the primary interstellar neutral atoms via the processes of electron-impact ionization, photoionization, and charge exchange with H^+ in the heliospheric interface. For the filtration factors of H and O we adopt the values 0.475 and 0.7, respectively, from Izmodenov et al. (1999).

Izmodenov et al. (1999) calculated the neutral density of primary interstellar neutral O as a function of radial distance between ~475 and 0 AU using a Monte Carlo method. They defined four regions with different plasma properties. We find that we can reproduce the neutral O densities in their paper at each interface of the four regions by assuming simple exponential attenuation due to the processes of electron-impact ionization, charge exchange with H^+, and photoionization, using reasonable plasma properties in each region. We then use the same plasma properties and the appropriate cross sections and rate coefficients for the reactions to calculate the filtration factors for the other atoms of interest, He, C, N, Ne, Na, Mg, Si, S, and Ar. The plasma properties we assumed for each region are guided by theoretical estimates (see, e.g., Izmodenov et al. 1999 and Zank et al. 2001a) and are given in Table 8.

TABLE 8

PLASMA PROPERTIES OF THREE REGIONS OF THE HELIOSPHERE

Region	Start (AU)	Stop (AU)	n_p[a] (cm^{-3})	v_{rel}[b] ($km\ s^{-1}$)	v_b[c] ($km\ s^{-1}$)	T (K)
VLISM → BS.....	475	320	0.07	11.5	25	8,000
BS → HP.....	320	170	0.17	25	25	20,000
HP → TS.....	170	90	0.0053	25	25	1.5×10^6

[a] Proton density, assumed to be the same as the electron density, n_e.
[b] Relative velocity of the interaction.
[c] Bulk velocity of the flow through the region.

For photoionization, we use the photoionization rates at 1 AU from Appendix A and assume the rate decreases with distance as $1/r^2$. The filtration factor across a region from radial position r_1 to r_2 due to photoionization, F_{ph}, is described by

$$\ln(F_{ph}) = -\frac{1}{v_b}\int_{r_1}^{r_2} \frac{\tau_1 dx}{x^2} \ , \tag{B1}$$

where v_b is the bulk flow velocity of the atoms through the region, τ_1 is the photoionization rate at 1 AU, and r_1 and r_2 are the boundary locations of the region.

For electron-impact ionization, we use the analytic representations of the rate coefficients as a function of temperature T from Voronov (1997). The rate coefficient is the Maxwellian-averaged product of the ionization cross section and electron velocity. The filtration factor due to electron-impact ionization, F_{ei}, is described by

$$\ln(F_{ei}) = -\frac{1}{v_b}\int_{r_1}^{r_2} \alpha(T) n_e \, dx \ , \tag{B2}$$

where $\alpha(T)$ is the electron-impact ionization rate coefficient at temperature T and n_e is the electron density.

For charge-exchange ionization, we use cross sections listed in Table 9 at two relative velocities from Table 8. The filtration factor due to charge exchange, F_{ce}, is described by

$$\ln(F_{ce}) = -\frac{1}{v_b}\int_{r_1}^{r_2} \sigma_Z n_p v_{rel} \, dx \ , \tag{B3}$$

where σ_Z is the charge-exchange cross section at relative velocity v_{rel} and n_p is the proton density, assumed to be the same as the electron density, n_e, in each region.

The filtration factors for each process were calculated across each of three regions, namely, from the unperturbed VLISM, assumed to be at 475 AU, to the bow shock (BS) at 320 AU, from the BS to the heliopause (HP) at 170 AU, and from the HP to the solar wind termination shock (TS) at 90 AU. The total filtration factor is the product of the three individual factors: $F_{tot} = F_{ph}F_{ei}F_{ce}$. The plasma properties were adjusted to get the same total filtration factor at three radial locations for primary O in Izmodenov et al. (1999), namely, 0.92 at the BS, 0.62 at the HP, and 0.49 at the TS.

In Table 10 we show the resulting filtration factors for primary interstellar neutral He, C, N, O, Ne, Na, Mg, Si, S, and Ar. The filtration factor of H is taken to be 0.475 (Izmodenov et al. 1999).

TABLE 9

CROSS SECTIONS FOR CHARGE EXCHANGE WITH H^+ IN HELIOSHEATH[a]

	CROSS SECTION[b]		
ELEMENT	At $v_{rel} = 11.5\ km\ s^{-1}$ (cm^2)	At $v_{rel} = 25\ km\ s^{-1}$ (cm^2)	REFERENCE
He.....	$<1 \times 10^{-21}$	$<1 \times 10^{-21}$	Barnett et al. 1990
C.....	2×10^{-21}	3×10^{-21}	Stancil et al. 1998
N	$<2 \times 10^{-17}$	$<2 \times 10^{-17}$	Kimura et al. 1997a
O.....	1.1×10^{-15}	1.0×10^{-15}	Stancil et al. 1999
Ne.....	$<1 \times 10^{-21}$	$<1 \times 10^{-21}$	Nakai et al. 1987
Na.....	$<1 \times 10^{-17}$	$<1 \times 10^{-17}$	Avakov et al. 1992
Mg.....	9×10^{-18}	7×10^{-16}	Allan et al. 1988
Si	1×10^{-15}	2×10^{-15}	Kimura et al. 1997a
S	2×10^{-17}	4.5×10^{-17}	Kimura et al. 1997b
Ar	$<1 \times 10^{-19}$	$<1 \times 10^{-19}$	Nakai et al. 1987

[a] For reaction $X + H^+ \rightarrow X^+ + H$.
[b] For He, N, Ne, Na, and Ar the estimates are based on an extrapolations from observations or calculations at higher energies.

TABLE 10

FILTRATION FACTORS AND INTERSTELLAR NEUTRAL DENSITIES[a]

ELEMENT	REGION VLISM → BS				REGION BS → HP				REGION HP → TS				REGION VLISM → TS				σ[d]	VLISM NEUTRAL DENSITY[b] (cm^{-3})
	F_{ce}	F_{ei}	F_{ph}	F_{tot}	F_{ce}[c]	F_{ei}	F_{ph}	F_{tot}	F_{ce}[c]	F_{ei}	F_{ph}	F_{tot}	F_{ce}[c]	F_{ei}	F_{ph}	F_{tot}		
He	1.00	1.00	1.00	1.00	1.00	1.00	1.00	1.00	1.00	0.95	1.00	0.94	1.00	0.95	0.99	0.94	0.02	$(1.7 \pm 0.2) \times 10^{-2}$
C	1.00	1.00	0.99	0.99	1.00	1.00	0.98	0.97	1.00	0.73	0.96	0.70	1.00	0.73	0.93	0.68	0.09	[e]
N	1.00	1.00	1.00	1.00	0.99	1.00	0.99	0.98	1.00	0.78	0.99	0.77	0.99	0.78	0.98	0.76	0.08	$(0.1 \pm 0.2) \times 10^{-5}$
O	0.92	1.00	1.00	0.92	0.68	1.00	0.99	0.67	0.99	0.81	0.99	0.79	0.62	0.81	0.97	0.70[f]	0.10	$(7.6 \pm 1.6) \times 10^{-5}$
Ne	1.00	1.00	1.00	1.00	1.00	1.00	0.99	0.99	1.00	0.90	0.99	0.89	1.00	0.90	0.98	0.88	0.04	$(8.6 \pm 1.7) \times 10^{-5}$
Na	1.00	1.00	0.97	0.96	1.00	0.42	0.92	0.38	1.00	0.64	0.85	0.54	1.00	0.27	0.75	0.20	0.08	[g]
Mg	1.00	1.00	1.00	1.00	0.77	0.66	0.99	0.50	1.00	0.47	0.98	0.46	0.76	0.31	0.97	0.23	0.09	[g]
Si	0.93	1.00	0.85	0.78	0.47	0.80	0.63	0.24	0.99	0.53	0.42	0.22	0.43	0.42	0.23	0.04	0.02	[g]
S	1.00	1.00	0.98	0.98	0.98	0.98	0.95	0.91	1.00	0.62	0.90	0.55	0.98	0.60	0.83	0.49	0.10	[g]
Ar	1.00	1.00	1.00	1.00	1.00	1.00	0.99	0.99	1.00	0.67	0.98	0.65	1.00	0.67	0.97	0.64	0.11	$(3.5 \pm 1.6) \times 10^{-7}$

[a] Filtration factor for H is taken to be 0.475 (Izmodenov et al. 1999) with an estimated uncertainty of 0.11, leading to VLISM neutral density of $(2.0 \pm 0.6) \times 10^{-1}\ cm^{-3}$.

[b] Derived from neutral densities estimated at the termination shock and filtration factors from this table.

[c] For He, N, Ne, Na, and Ar, we used upper limits for cross sections in Table 9.

[d] Uncertainties derived by assuming $\pm 20\%$ uncertainties on n_p, n_e, v_b, v_{rel}, τ_1, σ_z, α, and $\pm 10\%$ uncertainties on the radial positions of the boundary structures.

[e] Noninterstellar sources may contribute to observed ACR abundance.

[f] Product of factors in this table is 0.49, but for O there is a contribution from charge-exchange recombination of O^+ with H, leading to the filtration factor of 0.70 (Izmodenov et al. 1999) that we used in the analysis.

[g] Not likely of interstellar origin.

REFERENCES

Aldrovandi, S. M. V., & Péquignot, D. 1973, A&A, 25, 137
Allan, R. J., Clegg, R. E. S., Dickinson, A. S., & Flower, D. R. 1988, MNRAS, 235, 1245
Arnaud, M., & Rothenflug, R. 1985, A&AS, 60, 425
Avakov, G. V., Blokhintsev, L. D., Kadyrov, A. S., & Mukhamedzhanov, A. M. 1992, J. Phys. B, 25, 213
Barghouty, A. F. 2000, Phys. Rev. A, 61, 052702
Barghouty, A. F., Jokipii, J. R., & Mewaldt, R. A. 2000, in AIP Conf. Proc. 528, Acceleration and Transport of Energetic Particles Observed in the Heliosphere, ed. R. A. Mewaldt, J. R. Jokipii, M. A. Lee, E. Moebius, & T. H. Zurbuchen (Woodbury: AIP), 337
———. 2001, in The Outer Heliosphere: The Next Frontiers, ed. K. Scherer, H. Fichtner, H. J. Fahr, & E. Marsch (Amsterdam: Pergamon), 203
Barnett, C. F., Hunter, H. T., Kirkpatrick, M. I., Alvarez, I., Cisneros, C., & Phaneuf, R. A. 1990, Collisions of H, H_2, He and Li Atoms and Ions with Atoms and Molecules (Oak Ridge National Lab. Tech. Rep. ORNL-6086/V1)
Blandford, R. D., & Ostriker, J. P. 1978, ApJ, 221, L29
Cummings, A. C., & Stone, E. C. 1988, in Proc. 6th Int. Solar Wind Conf., Vol. 2, Composition, Gradients, and Temporal Variations of the Anomalous Cosmic-Ray Component, ed. V. J. Pizzo, T. Holzer, & D. G. Sime (Boulder: NCAR), 599
———. 1996, Space Sci. Rev., 78, 117
———. 1998, Space Sci. Rev., 83, 51
Cummings, A. C., Stone, E. C., & Steenberg, C. D. 1999, in Proc. 26 Int. Cosmic-Ray Conf. (Salt Lake City), 531
Ellison, D. C., Jones, F. C., & Baring, M. G. 1999, ApJ, 512, 403
Fahr, H. J., Ripken, H. W., & Lay, G. 1981, A&A, 102, 359
Fisk, L. A., Gloeckler, G., Zurbuchen, T. H., & Schwadron, N. A. 2000, in AIP Conf. Proc. 528, Acceleration and Transport of Energetic Particles Observed in the Heliosphere, ed. R. A. Mewaldt, J. R. Jokipii, M. A. Lee, E. Moebius, & T. H. Zurbuchen (Woodbury: AIP), 229
Fisk, L. A., Kozlovsky, B., & Ramaty, R. 1974, ApJ, 190, L35
Frisch, P. C. 1998, Space Sci. Rev., 86, 107
Geiss, J., Gloeckler, G., Fisk, L. A., & von Steiger, R. 1995, J. Geophys. Res., 100, 23373
Gloeckler, G., Fisk, L. A., Geiss, J., Schwadron, N. A., & Zurbuchen, T. H. 2000a, J. Geophys. Res., 105, 7459
Gloeckler, G., Fisk, L. A., Zurbuchen, T. H., & Schwadron, N. A. 2000b, in AIP Conf. Proc. 528, Acceleration and Transport of Energetic Particles Observed in the Heliosphere, ed. R. A. Mewaldt, J. R. Jokipii, M. A. Lee, E. Moebius, & T. H. Zurbuchen (Woodbury: AIP), 221
Gloeckler, G., & Geiss, J. 2001, in AIP Conf. Proc. 528, Acceleration and Transport of Energetic Particles Observed in the Heliosphere, ed. R. A. Mewaldt, J. R. Jokipii, M. A. Lee, E. Moebius, & T. H. Zurbuchen (Woodbury: AIP), 281
Goldstein, B. E., Neugebauer, M., Gosling, J. T., Bame, S. J., Phillips, J. L., McComas, D. J., & Balogh, A. 1995, Space Sci. Rev., 72, 113
Hamilton, D. C., Hill, M. E., Gloeckler, G., Decker, R. B., & Krimigis, S. M. 1999, in Proc. 26th Int. Cosmic Ray Conf. (Salt Lake City), 535
Izmodenov, V. V., Lallement, R., & Geiss, J. 1999, A&A, 344, 317
Jokipii, J. R. 1996, ApJ, 466, L47
Jokipii, J. R., & Kóta, J. 1989, J. Geophys. Res. Lett., 16, 1
Kimura, M., Gu, J., Hirsch, G., & Buenker, R. J. 1997a, Phys. Rev. A, 55, 2778
Kimura, M., Gu, J.-P., Hirsch, G., Buenker, R. J., Domondon, A., Watanabe, T., & Sato, H. 1997b, Phys. Rev. A, 56, 1892
Kimura, M., Sannigrahi, A. B., Gu, J., Hirsch, G., Buenker, R. J., & Shimamura, I. 1996, ApJ, 473, 1114
Kingdon, J. B., & Ferland, G. J. 1996, ApJS, 106, 205
Klecker, B., et al. 1995, ApJ, 442, L69
———. 1998, Space Sci. Rev., 83, 259
Kucharek, H., & Scholer, M. 1995, J. Geophys. Res., 100, 1745
Leske, R. A., Mewaldt, R. A., Christian, E. R., Cohen, C. M. S., Cummings, A. C., Slocum, P. L., Stone, E. C., von Rosenvinge, T. T., & Wiedenbeck, M. E. 2000, in AIP Conf. Proc. 528, Acceleration and Transport of Energetic Particles Observed in the Heliosphere ed. R. A. Mewaldt, J. R. Jokipii, M. A. Lee, E. Moebius, & T. H. Zurbuchen (Woodbury: AIP), 293
Mazzotta, P., Mazzitelli, G., Colafrancesco, S., & Vittorio, N. 1998, A&AS, 133, 403
Mewaldt, R. A. 1999, Adv. Space Res., 23, 541
Mewaldt, R. A., Selesnick, R. S., Cummings, J. R., Stone, E. C., & von Rosenvinge, T. T. 1996, ApJ, 466, L43
Nahar, S., Pradhan, A., & Zhang, H. 2001, ApJS, 133, 255
Nakai, Y., Shirai, T., Tabata, T., & Ito, R. 1987, At. Data Nucl. Data Tables, 37, 69
Pesses, M. E., Jokipii, J. R., & Eichler, D. 1981, ApJ, 246, L85
Reames, D. V. 1999, ApJ, 518, 473
Richardson, I. G., Barbier, L. M., Reames, D. V., & von Rosenvinge, T. T. 1993, J. Geophys. Res., 98, 13
Rucinski, D., Cummings, A. C., Gloeckler, G., Lazarus, A. J., Mobius, E., & Witte, M. 1996, Space Sci. Rev., 78, 73
Schwadron, N. A., & Geiss, J. 2000, J. Geophys. Res., 105, 7473
Schwadron, N. A., Geiss, J., Fisk, L. A., Gloeckler, G., Zurbuchen, T. H., & von Steiger, R. 2000, J. Geophys. Res., 105, 7465
Schwadron, N. A., Gloeckler, G., Fisk, L. A., Geiss, J., & Zurbuchen, T. H. 1999, in AIP Conf. Proc. 471, The Inner Source for Pickup Ions, ed. S. R. Habbal, R. Esser, J. V. Hollweg, & P. A. Isenberg (Woodbury: AIP), 487
Slavin, J. D., & Frisch, P. C. 2002, ApJ, 565, 364
Stancil, P. C., et al. 1998, ApJ, 502, 1006
Stancil, P. C., Schultz, D. R., Kimura, M., Gu, J.-P., Hirsch, G., & Buenker, R. J. 1999, A&AS, 140, 225
Stebbings, R. F., Smith, A. C. H., & Ehrhardt, H. 1964, J. Geophys. Res., 69, 2349
Steenberg, C. D. 2000, in AIP Conf. Proc. 528, Acceleration and Transport of Energetic Particles Observed in the Heliosphere ed. R. A. Mewaldt, J. R. Jokipii, M. A. Lee, E. Moebius, & T. H. Zurbuchen (Woodbury: AIP), 301
Steenkamp, R. 1995, Ph.D. thesis, Potchefstroom Univ.
Stone, E. C., & Cummings, A. C. 1997, in Proc. 25th Int. Cosmic-Ray Conf. (Durban), 289
Stone, E. C., Vogt, R. E., McDonald, F. B., Teegarden, B. J., Trainor, J. H., Jokipii, J. R., & Webber, W. R. 1977, Space Sci. Rev., 21, 355
Tabata, T., Ito, R., Nakai, Y., Shirai, T., Sataka, M., & Sugiura, T. 1988, Nucl. Instrum. Methods Phys. Res., 31, 375
Takashima, T., et al. 1997, ApJ, 477, L111
Tobiska, W. K., Woods, T., Eparvier, F., Viereck, R., Floyd, L., Bouwer, D., Rottman, G., & White, O. R. 2000, J. Atmos. Terr. Phys., 62, 1233
Vasyliunas, V. M., & Siscoe, G. L. 1976, J. Geophys. Res., 81, 1247
Verner, D. A., Ferland, G. J., Korista, K. T., & Yakovlev, D. G. 1996, ApJ, 465, 487
von Steiger, R., et al. 2000, J. Geophys. Res., 105, 27217
Voronov, G. S. 1997, At. Data Nucl. Data Tables, 65, 1
Witte, M., Banaszkiewicz, M., & Rosenbauer, H. 1996, Space Sci. Rev., 78, 289
Woods, T. N., et al. 1996, J. Geophys. Res., 101, 9541
Zank, G. P., Müller, H.-R., & Wood, B. E. 2001a, Phys. Plasmas, 8, 2385
Zank, G. P., Rice, W. K. M., Roux, J. A., & Matthaeus, W. H. 2001b, ApJ, 556, 494